

Revisiting the Anatomy of the Florisbad Hominin Cranium: Visualization of New Internal Features and Observations on Its Supposed Pathologies

ANTOINE BALZEAU*

PaleoFED team, UMR 7194, Histoire Naturelle des Humanités Préhistoriques, MNHN-CNRS-UPVD, Paris, FRANCE; and, Department of African Zoology, Royal Museum for Central Africa, Tervuren, Belgium; antoine.balzeau@mnhn.fr

JIAMING HUI

PaleoFED team, UMR 7194, Histoire Naturelle des Humanités Préhistoriques, MNHN-CNRS-UPVD, Paris, FRANCE; Key Laboratory of Vertebrate Evolution and Human Origins, Institute of Vertebrate Paleontology and Paleoanthropology, Chinese Academy of Sciences, Beijing 100044, CHINA; and, Sorbonne Université, Paris, FRANCE; jiaming.hui@etu.sorbonne-universite.fr

VICTOR GIOLLAND

PaleoFED team, UMR 7194, Histoire Naturelle des Humanités Préhistoriques, MNHN-CNRS-UPVD, Paris, FRANCE; victor.giolland@mnhn.fr

SHARON HOLT

Florisbad Quaternary Research Station, National Museum, Bloemfontein, 9301, SOUTH AFRICA; sholt@nationalmuseum.co.za

FREDERICK GRINE

Department of Anthropology and Department of Anatomical Sciences, Renaissance School of Medicine, Stony Brook University, Stony Brook, New York 11794, USA; frederick.grine@stonybrook.edu

corresponding author: Antoine Balzeau; antoine.balzeau@mnhn.fr

submitted: 8 October 2024; revised 30 December 2024; revised 13 March 2025; accepted: 25 April 2025

Handling Editor in Chief: Katerina Harvati

ABSTRACT

Among the Middle Pleistocene African fossils that are central to discussions about the evolution of *Homo sapiens* is the partial cranium from Florisbad, South Africa. The fossil, dated to MIS 8 (300–243 ka BP), combines some primitive traits that are shared with *Homo erectus* or *H. rhodesiensis* relative to *H. neanderthalensis* and *H. sapiens*, together with derived features shared with *H. sapiens* relative to *H. erectus*. It has been proposed that the specimen suffered from pathological conditions that resulted in an asymmetric and exaggeratedly thick vault together with external and internal lesions. Such pathologies could complicate anatomical comparison and attribution of the specimen. The purpose of the present work is to re-examine the calotte and provide new information on several aspects of its anatomy. We review the purported pathological conditions of the specimen, particularly those related to calotte asymmetry and the structural composition and thickness of the vault bone, employing micro-CT scan data, which also enabled description of the frontal sinuses, details relating to the diploic vessels and cerebral imprints on the endocranial surface. We compare several cranial traits seen in Florisbad with those observed in different hominin specimens. Detailed investigation of the supposed pathological traits of Florisbad reveals that they are all consistent with conditions observed for non-pathological living human and fossil hominin crania. The claim that pathology has altered the symmetry of the vault, as well as its thickness, distribution, and internal structure, is not supported. We also describe previously unreported aspects of anatomical features in which Florisbad differs from those observed exclusively in *H. sapiens*, including aspects of bone thickness distribution, the extension of the diploic system, and proportions of the endocast. Our results illustrate that in terms of cranial bone distribution and endocranial proportions, Florisbad most closely resembles the somewhat older Middle Pleistocene cranium from Kabwe 1, but it does not share the exceptionally large frontal sinuses seen in the Kabwe 1, Bodo, and Petralona crania. In sum, the results of this study suggest that the attribution of the Florisbad cranium to *Homo sapiens* may be unwarranted owing to the number of features in which it lacks the apomorphic states exhibited by our species.

INTRODUCTION

The purpose of the present work is to examine the Florisbad cranium in order to provide information on aspects of its anatomy, including several previously undocumented features. We review the putative pathological conditions of the specimen, particularly those related to calotte asymmetry and the bone thickness and the structural composition of the vault. In addition, we compare several cranial traits seen in Florisbad with observations for different hominin species in order to contribute to the discussion on the affinities of this Middle Pleistocene fossil.

Most genetic studies indicate that the earliest population divergence within *Homo sapiens* was between the ancestors of present-day Khoe-San and all other living populations (Veeramah and Hammer 2014) and this likely occurred sometime between ca. 200–100 ka (Chan et al. 2015; Gronau et al. 2011; Henn et al. 2018; Mallick et al. 2016; Ragsdale et al. 2023; Schiffels and Durbin 2014; Schlebusch et al. 2012; Song et al. 2017; Veeramah et al. 2012). However, these estimates are dependent on assumed parameters such as known germline mutation rates and generation time and, thus, even earlier divergence dates of 350–250 ka have been proposed (Scally and Durbin 2012; Schlebusch et al. 2017; 2020). A temporal range of ca. 350 to 100 ka BP would place the earliest population divergence within *H. sapiens* between the onset of Marine Isotope Stage (MIS) 10 at about 374 ka BP and the end of MIS 5d at about 100 ka BP (Bassinot et al. 1994; Imbrie et al. 1984; Lisiecki and Raymo 2005). Recent analyses have estimated the *H. sapiens* lineage to have split from the ancestor of the Denisovan – Neanderthal lineage between about 765–550 ka BP (Mafessoni and Prüfer 2017; Petr et al. 2020; Prüfer et al. 2014, 2017). Some authors suggest that the Sima de los Huesos hominin assemblage, possibly dated to around 430 ka (Pantoja-Pérez and Arsuaga 2024), should be subsumed within the Neanderthal record, which means that the paleogenetic divergence estimate significantly predates the earliest fossils.

In addition to the genetic evidence, the hominin fossil record provides evidence supporting the evolution of *Homo sapiens* in Africa (e.g., Galway-Witham and Stringer 2018; Hublin et al. 2017; Meneganzin et al. 2022; Pearson 2013; Scerri et al. 2014, 2018; Stringer 2016). However, there are also discussions about specimens that do not display the entire suite of *H. sapiens* apomorphies and about biological and taxonomic diversity in the Middle Pleistocene. Recently, several new *Homo* species have been proposed based on new discoveries or built on interpretation of the existing fossil record (e.g., *H. floresiensis*, *H. luzonensis*, *H. naledi*, *H. longi*, and *H. juluensis* (Bae and Wu 2024; Déroix et al. 2019; Hautavoine et al. 2024; Hurst et al. 2024; Kaifu et al. 2024; Ni et al. 2021; Roksandic et al. 2022)). Some of those taxa appear to be employed to replace the designation “archaic” *Homo sapiens* but ultimately do not help to resolve the question of the origin of our species. However, information obtained from the genetic diversity of current humanity concludes that our origin is indeed African, while the oldest fossil specimens indisputably attributed to our

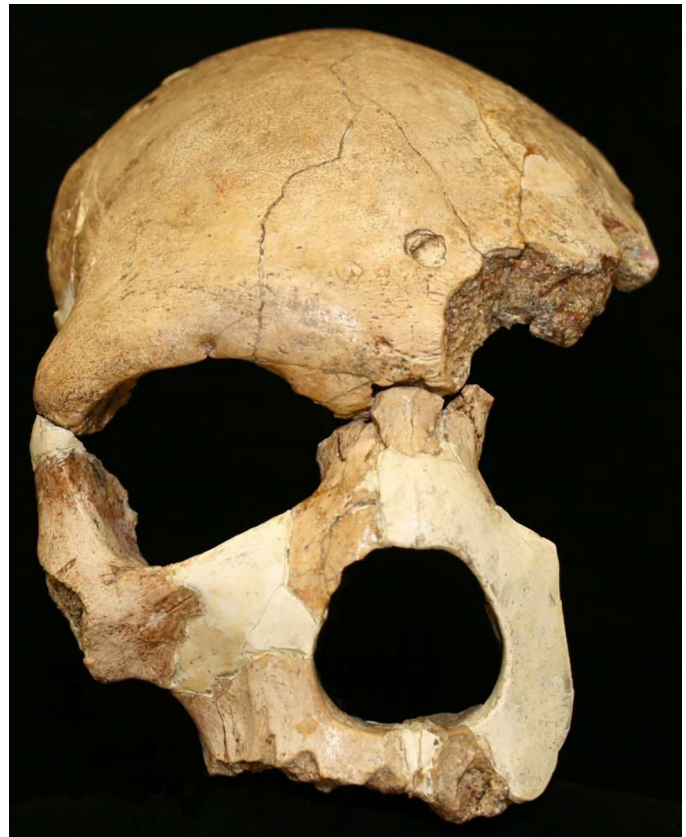


Figure 1. Facial view of the Florisbad cranium as reconstructed by Ron Clarke (1985).

species, from the Omo and Herto Bouri sites, come from this continent.

Among the Middle Pleistocene¹ African fossils proposed to have been involved in the evolutionary history of *H. sapiens* is the partial cranium from Florisbad, South Africa (Figure 1). It comprises a partial calotte (most of the frontal and portions of both parietals), a partial facial skeleton (much of the right zygomatic, some of the right maxilla, together with the frontal process and the incisive alveolus of the left maxilla), and an isolated right maxillary third molar (RM³).

The first artifacts and fossil bones at the site of Florisbad (28.76° S, 26.07° E), some 45km NW of the city of Bloemfontein, Free State, were discovered by Floris Venter, who owned the warm springs there and converted them to a recreational spa (Florisbad is Afrikaans for Floris' Bath). They were found in 1912 when Venter was digging to enlarge one of the spring baths and came to the attention of Robert Broom, who named two extinct species (*Cobus venteri* and *Connochaetes antiquus*) on them (Broom 1913). These finds prompted Dreyer to initiate excavations at the site in 1917, which were continued in 1926, 1928, and 1932. The hominin fossil was discovered in July, 1932 by Thomas F. Dreyer and Willeboer Venter (Dreyer 1938, 1947; Dreyer and Kappers 1935; Hoffman 1955; Meiring 1956).

GEOCHRONOLOGICAL AGE OF THE FLORISBAD CRANIUM

The pieces that constitute the hominin fossil derive from a saline warm water spring that vented through two stratigraphic horizons—the “Brown Sand” and “Peat 1” layers—from which optically stimulated luminescence (OSL) dates of 279 ± 47 ka and 281 ± 73 ka, respectively, have been obtained (Kuman 2023; Kuman and Clarke 1986; Kuman et al. 1999; Toffolo 2024). Additionally, enamel from the hominin RM³ has been dated with electron spin resonance (ESR) to 259 ± 35 ka BP (Grün 2006; Grün and Stringer 2023; Grün et al. 1996). As such, there is reasonable concordance among the age estimates for the Florisbad cranium, although all must be regarded with some reservation owing to uncertainties around the site’s reconstructed radioactive environmental history. However, Pinder (2021) has demonstrated that single grain OSL readings from a separate excavation pit at Florisbad show good agreement for many of the MSA samples reported earlier, indicating that sedimentation at the site occurred from >254 ka BP into the Holocene, with a relatively recent hiatus that lasted approximately 100,000 years. Pinder (2021) noted that her data agreed with the previously reported ESR age for the hominin M³.

Berger and Hawks (2023) have recently suggested that the ESR age estimate from the molar may not pertain to the cranium itself. However, the only stratigraphic horizons from which the cranium and the tooth could have derived and the M³ itself have concordant dates. In addition, the degree of occlusal attrition on the molar crown detailed by Smith et al. (2015) is consistent with the full endocranial and partial ectocranial fusion of the coronal and sagittal sutures in indicating an advanced adult ontogenetic age for this individual. Moreover, both Berger and Hawks (2023) and Grün and Stringer (2023) are in error when they state that the maxillary fragment does not preserve the portion that could confirm or reject a physical conjoin with the tooth, and that the molar cannot be fitted to the cranium directly. As noted by Grine et al. (2019: 151), the alveolar margin of the right maxilla has suffered taphonomic loss from the canine to the M² (it is not resorbed, contrary to Curnoe and Brink [2010]; rather it has been chewed away, probably by the same carnivore that left its canine puncture marks on the frontal [Tappen 1987]). However, the roof and part of the mesial wall of the RM³ socket are preserved, and the molar root fits comfortably in it (Grine et al. 2019: 151). Therefore, as noted by Grün and Stringer (2023: 37), the molar is “most likely part of the same individual, considering that all other human bone fragments seem to be,” and that “it is the only dental material that can unequivocally be associated with the human bones.” Thus, there is currently no reason to doubt that the Florisbad cranium likely dates to MIS 8 (i.e., between 300–243 ka BP [Lisiecki and Raymo 2005]).

EVOLUTIONARY INTERPRETATIONS OF THE FLORISBAD CRANIUM

The Florisbad cranium was attributed by Dreyer (1935) to the species *Homo (Africanthropus) helmei*, named after

Captain R. Egerton Helme, who had provided funding for Dreyer’s excavations. It is consistently identified as a form that was a potential source population for *H. sapiens* (e.g., Bruner and Lombard 2020; Clarke 1985; Rightmire 1978, 1984; McBrearty and Brooks 2000; Mounier and Lahr 2019; Smith et al. 1989), or as an ‘archaic’ member of *H. sapiens* (e.g., Bräuer 2008; Bräuer and Rimbach 1990; Hublin et al. 2017; Stringer 2016). Some workers recognize *H. helmei* as a potentially distinct taxon but they note that “*H. helmei* is a somewhat problematic taxon, as there is as yet no formal diagnosis for the species and its unique autapomorphies are not defined... *H. helmei* may be expected to exhibit a mix of primitive and derived features” (McBrearty and Brooks 2000: 480).

The cranium shows a well-developed supraorbital torus, a broad face, a thick cranial vault, and a pattern of restricted meningeal vascularization (Bruner and Lombard 2020; Rightmire 1978; Singer 1958; Tobias 1968) in which it resembles the crania from Kabwe and Saldanha (Bruner and Lombard 2020; Clarke 1985; Rightmire 1978). Clarke (1985: 302) also noted the presence of “an extensive frontal sinus measuring 31.5 mm laterally and 21 mm posteriorly.” At the same time, however, the cranium exhibits a number of derived traits that approximate the condition observed in *H. sapiens*, such as a rather vertically domed (bulging) frontal, a relatively high and rounded cranial vault, a distinct maxillary canine fossa, and an incipiently divided supraorbital torus (Bruner et al. 2013; Galloway 1937; Rightmire 1978; Stringer and Andrews 1988).

There has been some disagreement over details of Florisbad’s facial morphology owing to its fragmentary nature and to the various pieces having been reconstructed in different configurations by Dreyer and Kappers (1935), Clarke (1985) and Schwartz and Tattersall (2003). The problem, as noted by Clarke (1985), is that there are no positive joins between the major facial elements. Measurements recorded from these different reconstructions will undoubtedly affect the results of comparisons with other hominin fossils and modern human samples.

TAPHONOMIC DAMAGE TO THE FLORISBAD CRANIUM

The specimen has suffered from postmortem or perimortem taphonomic damage. As noted by Clarke (1985), there are several tooth puncture marks on the frontal, including a large punctate depression from a carnivore tooth posterior to glabella and chewing marks along the left side of the calotte. In addition, the left supraorbital margin has been gnawed away, as has the lateral alveolar margin of the right maxilla.

Finally, a large (27mm²) piece of the right parietal just posterior to the coronal suture was removed by Protsch (1975: Table 1).

PATHOLOGY OF THE FLORISBAD CRANIUM

Pathological conditions have been convincingly demonstrated to have affected several hominin crania from the Middle - Late Pleistocene of Africa, including those from

Singa, Sudan (Brothwell 1974; Spoor et al. 1998; Stringer et al. 1985), Salé, Morocco (Hublin 1985, 2009) and Eliye Springs, Kenya (Bräuer et al. 2003). The identification of paleopathology is of importance beyond a basic interest in the expression of disease in hominin fossils, as an appreciation of its potential impact on cranial morphology is crucial in assessing their morphological affinities (e.g., Spoor et al. 1998). This is, indeed, relevant in the three cases noted above. Hublin (1985, 2009) has inferred that the Salé individual suffered from congenital torticollis related to an abnormal (deformed and asymmetrical) planum nuchae, and that the latter has impacted morphometric assessments that include the occipital. Similarly, the Singa 1 specimen has been suggested to display morphological resemblance to a recent African population, with its accentuated parietal bossing interpreted by early workers as indicating Khoesan affinities (Wells 1951; Woodward 1938). However, this feature appears to be unduly developed owing to the cranium's asymmetry and underlying pathology (Brothwell 1974; Spoor et al. 1998; Stringer et al. 1985). The partial cranium from Eliye Springs (KNM-ES 11693) has a highly porotic ectocranial surface and greatly exaggerated vault thickness, which likely affects its overall morphometric assessment (Bräuer et al. 2003).

Curnoe and Brink (2010) argued that the Florisbad cranium exhibits numerous pathological conditions, including among others: 1) an asymmetrical vault; 2) thick cranial vault bones with pathological expansion of the diploë; 3) internal neurocranial lesions and irregular depressions; 4) external neurocranial lesions; 5) cribra orbitalia; and 6) dentoalveolar lesions affecting the incisor and canine alveoli. Previously, Schwartz and Tattersall (2003: 81) described its anterior palatal depth as probably having been affected by “bony resorption due to abscessing” of the right maxilla in the region of the canine. We agree that resorption has affected the anterior alveolar margin in the region of the incisors and canines; however, its most dramatic manifestation is in the form of an abscess cavity associated with the I² alveolus.

The endocranial aspect of the calotte shows relief that corresponds to impressions from the cerebrum and the blood circulation between the brain and skull. In addition, Pacchionian depressions (the variably shallow pits in the inner table of the vault produced by the arachnoid granulations which typically protrude into the superior sagittal [dural] venous sinus and contribute to cerebrospinal fluid reabsorption) are visible, as is the course of the sagittal sinus and imprints of the anterior and middle meningeal arterial systems. Curnoe and Brink (2010) considered a number of these features to be related to pathological lesions. An exhaustive review of the evidence proffered by them relating to the multitude of pathological conditions that they envisioned affecting the Florisbad fossil is beyond the scope of this study.

Some aspects, such as the suspected presence of cribra orbitalia, even if correctly diagnosed, are of little importance in view of the fact that the porosity that defines cribra orbitalia (*sensu stricto*) is a normal vascular / developmental

phenomenon (Cole and Waldron 2019; Rotschild et al. 2021; Zdilla et al. 2022). Indeed, cribra orbitalia is present in over 12% of recent North American and nearly 17% of South African adults (and in 40% of North American and 25% of South African juveniles) (Steyn et al. 2016).

In this context, we aim to provide a more accurate appreciation of the anatomy and morphology of this fossil by concentrating on the more salient features described by Curnoe and Brink, namely: 1) the asymmetry of the cranial vault, 2) the thickness of the vault bones and the pathological expansion of the diploë, and 3) the presence of internal neurocranial lesions and irregular depressions. Because these purported pathologies could affect the general anatomy of the specimen, it is important to establish their validity before investigating other anatomical details of the fossil. We also examine in detail the Florisbad cranium in order to provide information on several aspects of its anatomy, including several previously undocumented features.

MATERIALS AND METHODS

IMAGING DATA ON THE FOSSIL

The Florisbad cranium was examined over a period of two weeks at the National Museum, Bloemfontein in February, 2011 by one of us (FEG) aided by a 10x Triplet geological hand lens and a Leica M Series Stereo Zoom microscope. The cranium and molar were micro-CT scanned by two of us (FEG and SH) at the Stellenbosch University CT Scanner Facility (du Plessis et al. 2016) in 2018. The facial and calotte portions of the cranium were scanned separately as was the third molar using the General Electric Phoenix VTOMEX L240 micro-computed tomography (μ CT) system. We employed a current of 880 μ A and an accelerating voltage of 170kV. Voxels are isometric (same size in the three dimensions) and measure 0.0125mm³ for the cranial bones and 0.0136mm³ for the molar. X-ray projection images were acquired at between 2300–65000 steps during a full rotation of the sample. At each step position, the first image was disregarded, and the subsequent three images averaged to produce higher quality images than standard. A detector shift was activated to minimize ring artifacts. The resulting micro-CT scan data were visualized using Avizo 7 and Volume Graphics VGSTUDIO MAX 3.1.

Curnoe and Brink (2010) employed standard medical grade CT scans recorded at the Bloemfontein MediClinic in 2008. These scans had relatively low resolution (0.625mm³ voxel size at 140kV and 400mA). As such, they are not optimized to illustrate bone structure at the level of details they describe (at the nearest 0.1mm). In this context, our imaging dataset should aid in determining whether the traits previously described are pathological. We utilized micro-computed tomography (μ CT) to overcome the modest resolution of medical grade CT scans in order to provide a detailed assessment of the anatomy of the vault of the Florisbad cranium. In particular, we: 1) measured the thickness and structure (i.e., respective thickness of the internal table, the diploic layer, and the external table) of the cranial vault, 2) visualized the diploic channels within the

vault bones, 3) examined the surface of the endocast, as reconstructed from the endocranial surface of this specimen, and 4) visualized the compartments of the frontal sinus.

CRANIAL VAULT THICKNESS AND COMPOSITION

A reassessment of the position of the median sagittal plane enables an evaluation of the supposed vault asymmetry observed by Curnoe and Brink (2010).

We measured the overall thickness and composition (i.e., respective thickness of the internal table, the diploic layer, and the external table) of the cranial vault at selected points to evaluate the claim by Curnoe and Brink (2010) that vault thickness was altered by its pathological condition. A crucial methodological point is that thickness can only be quantified accurately on either 2D CT or micro-CT slices but also in 3D (e.g., Copes 2016) when measurements are recorded perpendicular to the vault. Curnoe and Brink (2010) used oblique slices and therefore their measurements cannot be repeated. Therefore, we followed Balzeau (2007) in employing the median sagittal plane as the reference by which repeated measurement of bone thickness could be assessed along its length. This protocol permitted the measurement of cranial vault thickness (CVT) and vault composition at bregma and the center of the frontal bone in the median sagittal plane. Those two points were also employed by Curnoe in his study. We also recorded thickness measurements at the center of the right parietal bone by reconstructing a slice perpendicular to the midsagittal plane that passes through the selected location on the parietal. This slice was selected to cross this point with an orientation perpendicular to bone thickness to enable accurate measurements. This modification of our protocol permits comparison of our measurements with those obtained at a supposedly similar point to that used by Curnoe and Brink (2010). Finally, we could not repeat the measurement at two of the other locations used by Curnoe and Brink. In the first instance, the actual location of the landmark they identified as “frontal squama” was not clearly defined, so we could not repeat it. Moreover, because several cracks run along the right side of the frontal squama, the different layers of bone cannot be reliably identified in this area. In the second instance, we did not measure thickness at the so-called ‘mid-sagittal suture’ as defined by Curnoe and Brink (2010) for three reasons. The first relates to the fact that they misidentified the median sagittal plane, and the second to the fact that the remnant suture is present endocranially, which precludes measurement of the internal layer of bone. The antero-posterior location of the point is not detailed by them, so we cannot identify the position of the measurement they recorded.

Bone thickness can also be quantified using a second approach that entails measurement over a larger anatomical area than at specific landmarks. Following Balzeau (2013), we delimited a parasagittal region that extended several centimeters on either side of the median sagittal plane with parallel borders running posteriorly from a postorbital line that delineated the section at which vault thickness was no

longer influenced by the supraorbital structures (see Balzeau 2013: Figure 1). Although the limits of the region of interest are not perfectly reproducible on all crania included in the comparative sample, cranial vault thickness distribution can be generated and represented by colormaps and directly compared to the description by Curnoe and Brink. The colormaps were generated following published protocols (Balzeau 2013; Balzeau and Charlier 2016; Balzeau et al. 2017; Beaudet et al. 2022; Hui and Balzeau 2024). The ‘SurfaceDistance’ algorithm of Avizo v9.0 was used to automatically calculate the distance between the ecto- and endocranial surfaces for regions of interest. The range of the color scale was adjusted to highlight thicknesses ranging between 2mm and 22mm for comparison with previously published data (Balzeau 2013; Balzeau et al. 2017). The colormaps were displayed on the ectocranial surface. The resulting data for Florisbad are compared to the results published by Balzeau (2013; Balzeau et al. 2017) to examine the distribution and asymmetry of CVT in a comparative framework. The comparative samples are the same as employed by Balzeau (2013) and are detailed in Table S1. They comprise fossils attributed to *H. erectus*, *H. neanderthalensis*, and fossil *H. sapiens*. The recent *H. sapiens* sample comprises 20 male and 20 female crania from Europe.

The diploic channels within the cranial vault bones were described following Hui and Balzeau (2023), where the 2D tomographic images of the Florisbad cranium were inspected slice by slice in 3D Slicer (v4.13) and the 3D cranial model was rendered transparent to observe its embedded diploic structures. By visually inspecting the 2D images and the transparent 3D models, we located diploic cavities in the shape of vessels, which are regarded as the channels that housed the diploic venous network. The diploic channels were segmented manually using the ‘Paint’ function in 3D Slicer. The segmented diploic channel models were displayed inside the transparent cranial model to investigate their distribution and drainage routes. The following analysis of Florisbad diploic channels reused the data from Hui (2024). Comparative information was available for fossil *H. sapiens* and *H. neanderthalensis*, as well as for several other specimens attributed to *H. erectus* and *H. naledi* (Hui 2024). The list of the specimens is provided in Table S1.

ENDOCRANIAL ANATOMY

With reference to the surface of the Florisbad endocast, we restrict our analysis to features that are clearly visible and that we could interpret with a high level of confidence based on our previous experience (e.g., Hui et al. 2025; Hurst et al. 2024; Labra et al. 2024). Because the endocranial surface of this specimen is incomplete, we have reconstructed the virtual model of the left lateral wall of the frontal lobe using the preserved area on the right to enable morphometric comparisons. The mirrored surface was aligned on the preserved anatomical area on that side. Doing so allowed us to estimate the position of the missing third frontal convolution on the left side. Figure 2 shows the actual preservation of the specimen and illustrates that only minor reconstruction was necessary to locate this landmark. The frontal

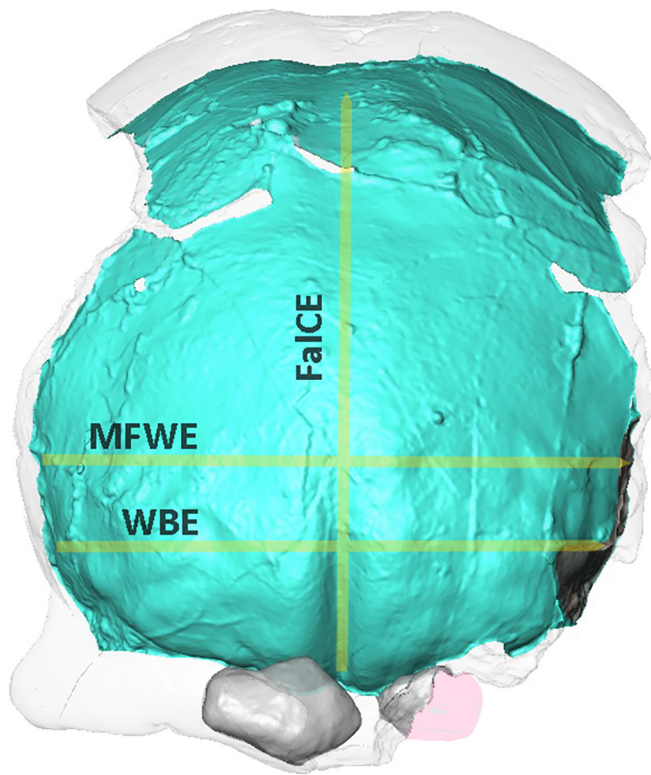


Figure 2. Illustration of the minimal reconstruction of the frontal lobes to measure three endocranial distances (lines in yellow) and of the lateral extension of the left frontal sinus to estimate its dimensions (the hollow red area is a raw estimation of its extension).

lobes of the endocranium were measured using the available landmarks of the frontal beak, the bilateral points on the Broca's cap, the points at the maximal width of the frontal lobe, and the intersection of the central sulci. As such, the frontal cord that extends between the frontal beak and the junction of the central sulci (denoted FaICE), the width at the Broca's cap (denoted WBE), and the maximum width of the frontal lobes (denoted MFWE) can be measured (see Figure 2). Morphometric data for Florisbad and the comparative samples of fossil hominins and recent humans were scaled using their respective endocranial volumes (EV) according to the formula $((x_i / (3\sqrt{EV_i}) * 100))$. The value for Florisbad is from the literature (Bruner and Lombard 2020). Even if the specimen is not complete, the use of the cube-root of the volume limits the influence of the approximation in the estimation of the complete volume. Principal component analyses (PCA) were performed on the variance-covariance matrix of the three absolute dimensions (FaICE, WBE, and MFWE) and for those variables scaled using their respective endocranial volume.

Univariate analyses were carried out using the adjusted z-score (Azs) (Scolan et al. 2011), in which 95% of the variation of the reference population is included between -1 and $+1$. An Azs lower than -1 or higher than $+1$ is beyond 95% of the variation of the reference sample. The comparative samples used here are the same as in Hurst et al. (2024)

and include specimens of australopiths, *H. sapiens*, *H. neanderthalensis*, and *H. erectus*, as well as specimens for which specific attribution is debated (LH 18, Kabwe 1, and Djebel Irhoud 1). The details are given in Table S1. Early hominins (e.g., australopiths) are included because they inform on the size and shape of the endocranial cast in ancient fossils and help to distinguish later groups. Specimens with a debated taxonomic attribution are included as they can provide important comparative information about Florisbad.

FRONTAL PNEUMATIZATION MORPHOLOGY AND DIMENSIONS

Finally, we investigated the frontal sinus in order to describe its morphology, and to compare its reconstructed volume with the sizes of those in other Middle and Late Pleistocene African hominin crania. Because the left supra-orbital region is almost entirely missing, and the inferior walls (limits) of the air cells in the bregmatic region and the adjacent right supraorbital torus are lacking (Figure 3), we measured the volumes of these cavities as preserved and as reconstructed by us utilizing the contours of the surrounding bone (see Figure 2).

3D reconstruction of the sinuses and assessment of the volumes were performed using the methods detailed by Balzeau et al. (2017; 2021) and Butaric et al. (2022). Segmentation was done manually with Avizo 7.0. We recorded 8 linear measurements on the 3D models of the sinuses (Table 1) as defined by Balzeau et al. (2022) in order to perform a linear discriminant analysis (LDA) to facilitate comparison between Florisbad and other specimens listed in Table S1. The bilateral measurements were combined together to provide a maximal extension of the total pneumatization in some directions. A total of 11 variables quantify sinus size and shape. Comparative samples for this analysis contain 94 specimens from most hominin species and 105 recent *H. sapiens* (Balzeau et al. 2022). The groups were early hominins (N=12), *H. erectus* (N=14), *Homo neanderthalensis* (N=21), and *H. sapiens* (N=105). It should be noted that these linear measurements were not utilized in the reconstruction of the volume of the frontal sinus. Moreover, the description of the preserved area of the sinuses is by itself informative of the anatomy of this pneumatization. Because the inferior margins of the sinus on the left side are incomplete, some of the dimensions required estimation. Our measurements were taken on the 3D models and correspond to the overall extension of pneumatization in space. Thus, a small break or a missing area does not necessarily affect the overall maximum extension in one direction. As a result, the protocol we used permitted direct measurement of 5 of the 8 measurements that are not affected by incomplete preservation on Florisbad. Estimation of the other 3 variables (Width, ALL, and SLI) was based on the shape of the preserved area and on the configuration of the cell on the left compared to that on the right side to estimate the extension of the missing area. Indeed, only minimal estimation of the missing area of the sinus (as visible on Figure 2) was necessary to estimate the linear dimensions in 3D as defined for our protocol. Measurements were repeated to ensure

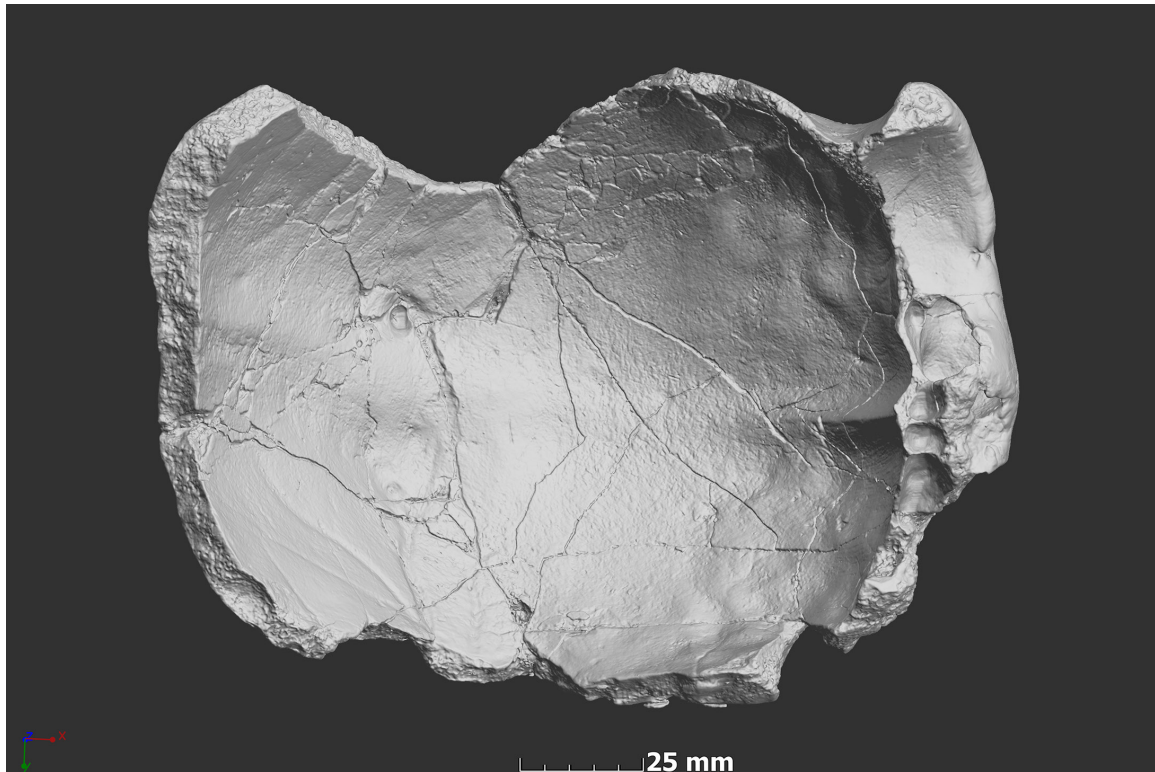


Figure 3. Internal view of the Florisbad calotte (anterior is to the right). Note the open inferior borders of the frontal sinus cavities in the glabellar and supraorbital moieties (on the right) and the unmistakable development of the internal frontal crest. This is a 3D surface volume rendering from the micro-CT scan of the specimen.

TABLE 1. DEFINITIONS OF THE MEASUREMENTS RECORDED FOR THE FRONTAL SINUS OF THE FLORISBAD CRANIUM (see Balzeau et al. 2022 for details of the method).*

Measurement	Abbr.	Definition	View
Width	W	Maximum lateral extension of pneumatization	Anterior
Height	H	Maximum superoinferior height of pneumatization	Anterior
Anterior length (left)	ALl	Maximum inferomedial to superolateral length of left sinus	Anterior
Anterior length (right)	ALr	Maximum inferomedial to superolateral length of right sinus	Anterior
Anterior length	2AL	ALl + ALr	Anterior
Superior length (left)	SLl	Maximum mediolateral extension of left sinus	Superior
Superior length (right)	SLr	Maximum mediolateral extension of right sinus	Superior
Superior length	2SL	SLl + SLr	Superior
Antero-posterior length	AP	Anteroposterior length	Lateral (left)
Antero-posterior length 2	AP2	Most anterior point to most superoposterior point	Lateral (left)
Combined AP length	2AP	AP + AP2	Lateral (left)

*Definitions in italics correspond to the dimensions that were estimated for Florisbad.

that no important error was made. This reconstruction concerned only its maximal extension to ensure the feasibility of our linear measurement. This approach was mandatory as the asymmetry in the extension of the pneumatization in this specimen (see Figure 2) made doubling the values observed on the preserved side to estimate frontal sinus size and shape in Florisbad a poorer proxy than our estimation that takes into account this parameter.

The three estimated dimensions relate to the anterior and superior lengths of the left sinus (variables ALI and SLI) as well as the total width of the frontal sinus (W) because the lateral extent of the left sinus is not preserved. The height and antero-posterior dimensions are not affected by the incomplete preservation of the left sinus. Indeed, the preserved medial border of the left sinus shows that both its vertical and AP extensions are more restricted than on the right and therefore that those dimensions can be measured directly on the preserved areas of pneumatization. Indeed, the right side is informative of the global extension of the whole pneumatization in those orientations. To estimate the lateral extension of the left sinus we compared it to the right side, where the sinus extends to a point just medial to the most elevated point of the orbit. A similar lateral position on the left side was used to estimate the left anterior and superior length (ALI and SLI, respectively) and the total width (W) of the sinuses. Based on the preserved shape of the sinuses and the general symmetry of the extension of the sinuses observed in our comparative samples, it is highly likely that the global extension of the sinuses was included within the extension that we have estimated. Although these variables are approximations, the globular shape of the sinus renders our estimation of its original size very likely. The dimensions are very unlikely to have been much larger than estimated here because the available areas in the frontal bone would not have permitted a much larger expansion of the pneumatization. Because all the linear measurements were used in the linear discriminant analyses and because of the limited impact of incomplete preservation in relation with our protocol, the estimates for the three variables likely had limited impact on the results and the interpretation of the position of Florisbad within the large comparative context.

Finally, the volume of the right and left sinuses was calculated by measuring the volume of the pneumatization that is preserved on the specimen and estimating the volume of the missing part. We estimated that approximately two-thirds of the total volume of the sinuses was preserved based on the relative sizes of the preserved parts of the left and right sinuses, their globular shapes, and our experience with large numbers of fossil and recent human sinuses (Balzeau et al. 2022; Greening et al. 2023; Grine et al. 2024). So, our estimation of the volume corresponds to the preserved volume multiplied by 3/2. Although this is an estimation, this imprecision does not have a significant impact on our comparisons when we employ the cube-root of the estimated volume in this analysis.

RESULTS

DETAILED ANATOMICAL DESCRIPTION OF THE FLORISBAD FOSSIL

The results of our analyses of the Florisbad cranium are presented in relation to: 1) the proposed asymmetry of the cranial vault, 2) the thickness and composition of the vault bones, 3) the identification of diploic channels within the vault, 4) the endocranial anatomy, and 5) the shape and volume of the frontal sinus.

Cranial Vault Asymmetry

Curnoe and Brink (2010: 505) state that “the Florisbad vault is both thick and asymmetrical in its thickness,” noting that “this is especially clear along the posterior course of the parietal bones where the calvaria have been broken post-mortem” and directing the reader to contrast the left and right sides of the parietal vault illustrated in their Figure 2A, reproduced here as Figure 4A. According to its legend, the white arrow indicates the sagittal suture. However, it is clear the white arrow is placed some 17.3mm to the left of the median sagittal plane. This plane, and hence the placement of the sagittal suture can be ascertained by inspection of the endocranial aspect of the specimen (see Figures 3 and 4), where some 25mm of the frontal crest is preserved. The frontal crest, which serves as the attachment of the midline dural reflection, the falx cerebri, corresponds to the median sagittal plane (Figure 4B, dashed line). Successive coronal sections through the parietals just anterior to the fractured posterior margin (Figure 4C) and just posterior to the coronal suture (Figure 4D) reveal the symmetry of the two sides of the cranium and in the distribution of its thickness across the preserved elements. In fact, Curnoe and Brink misidentified the midline as being coincident with a postmortem crack.

Cranial Vault Thickness and Composition

A superior view of the calotte (Figure 5) reveals the presence of a median sagittal depression (the “interparietal groove”) that was first observed by Galloway (1937). Habgood (1989) also noted it, as did Bruner and Lombard (2020), who suggested that it might be related to a reduction of the diploë in the midsagittal region. Habgood (1989: 18) regarded the presence of an interparietal groove as a “Khoisan feature,” presumably because it had been identified on a number of Later Stone Age crania from the Cape coastal belt of South Africa by earlier studies (e.g., Cassel et al. 1942; Galloway 1936; Grobbelaar and Goodwin 1952; Kohler 1942; Laing 1929). However, this depression occurs in relatively high frequency (ca. 36%) in other recent sub-Saharan African populations (de Villiers 1968) and Shore (1938) has recorded its presence in 12% of recent Egyptian crania. This feature has only limited (if any) impact on the cranial vault thickness variation in this area, which does not show a decrease in total bone thickness (Figure 6).

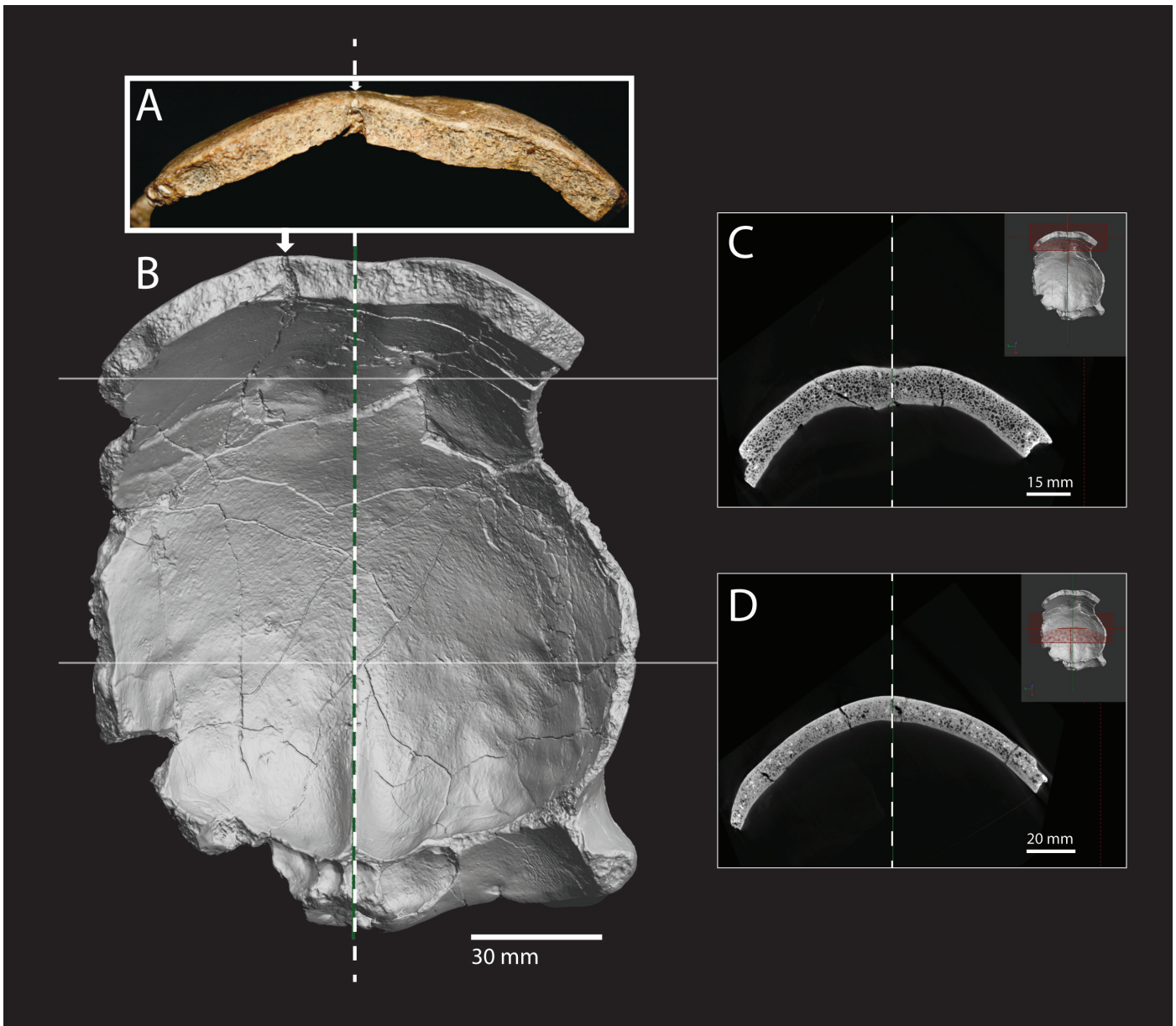


Figure 4. Demonstrating the lack of asymmetry affecting the cranial vault of the Florisbad specimen. A) Curnoe's orientation of the vault at its posterior broken margin with the white arrow indicating his identification of the median sagittal plane (from Curnoe and Brink 2010: Figure 2); B) the 3D surface volume rendering of the internal aspect of the calotte, the green dashed line is coincident with the frontal crest and identifies the median sagittal plane, the white arrow is Curnoe and Brink's identification of the median sagittal plane; C) micro-CT scan cross-section through the parietal bones just anterior to the broken margin at the back to the coronal suture (the plane of section is indicated by the red hatch plane in the inset); D) micro-CT scan cross-section through the parietal bones just posterior to the coronal suture (the plane of section is indicated by the red hatch plane in the inset).

Curnoe and Brink suggested that the distribution of the cranial vault bone thickness in the Florisbad cranium was asymmetrical. However, the heat map representing the distribution of bone thickness does not reveal any remarkable variation in CVT between the right and left parietal bones nor in the frontal bone (see Figure 6). Accordingly, the general distribution of CVT is rather homogeneously distributed between both sides over the preserved areas of calotte.

Concerning the variation in different parts of the calotte, the pattern of distribution shows a thickening along the course of the internal frontal crest, around the bregmatic area and along the median sagittal plane at the junction of the parietal bones. Restricted thinning of the frontal bone corresponds to the locations of the middle and superior frontal gyri as observed on its endocranial surface. Regions of minimum CVT (displayed in white and light blue

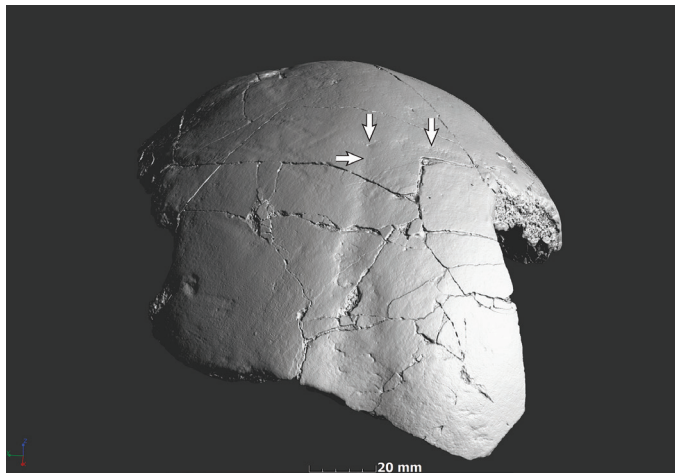


Figure 5. Posterosuperior view of a 3D surface volume rendering of the Florisbad calotte. Note the rather prominent interparietal depression at the back and the partial remnants of the sagittal (white arrow on the left) and coronal (white arrow on the right) sutures.

in Figure 6) are located in the medial parts of the ascending frontal gyri where arachnoid (Pacchonian) granulation pits are present.

The bone thickness values at key locations of the calotte—bregma, midfrontal median sagittal plane and mid-parietal right side—are presented in Table 2. Some of the absolute values differ from those reported by Curnoe and Brink, and this is most likely due to differing definitions of the points at which the measurements were recorded. For example, while we measured thickness at bregma, Curnoe and Brink (2010: 506) recorded it a point “near bregma, measured just posterior to bregma.” Our measurement of thickness at bregma is 11.6mm as compared to 8.5mm in Curnoe and Brink (2010: 506), and our mid-parietal point differs from their “parietal mid-external sur-

face” (8.8mm vs. 10.8mm). However, we obtain similar values for the mid-frontal point in the median sagittal plane (11.3mm vs. 11mm), which further reflects the symmetry of the frontal as their point is some 17mm from the actual median sagittal plane. Additionally, pixel size for the data collected by Curnoe and Brink (2010) is 0.625mm, and this degree of resolution does not allow precision beyond the nearest 0.5mm. Finally, our quantification at specific points is consistent with the values observed through the color-map of bone thickness distribution.

An important consideration is that overall vault thickness may be related to its compositional structure involving the internal table, external table, and diploic layer (Figure 7). At the three locations defined above (bregma, mid-frontal point, and mid-parietal point), we find that the proportion of the diploë relative to the total thickness varies between 63% and 75% (see Table 2). Although Curnoe and Brink (2010) reported values of between 67% and 86%, it should be noted that their measurement of thickness recorded to the nearest 0.1mm, including, for example, a value of 0.1mm for the external table at two locations. However, this is methodologically unattainable with a resolution of 0.625mm³ because theoretically, measurement error cannot be less than half the size of the pixels. It is clear from their published figures that the image quality is clearly not sufficient to adequately and precisely delimitate the three components of the vault thickness.

Moreover, Curnoe and Brink assessed cranial thickness on parasagittal sections that were not perpendicular to bone thickness (Figure 8), which results in an artificial increase of bone thickness values. This explains the discrepancy between at least some of the measurements recorded by them and by us. Our use of specific landmark and methodological protocols (i.e., using orthogonal images to quantify CVT and by mapping thickness variation) and the use of higher resolution images mean that our measurements more accurately reflect the characteristics of the vault of this specimen compared to the data published by Curnoe and Brink.

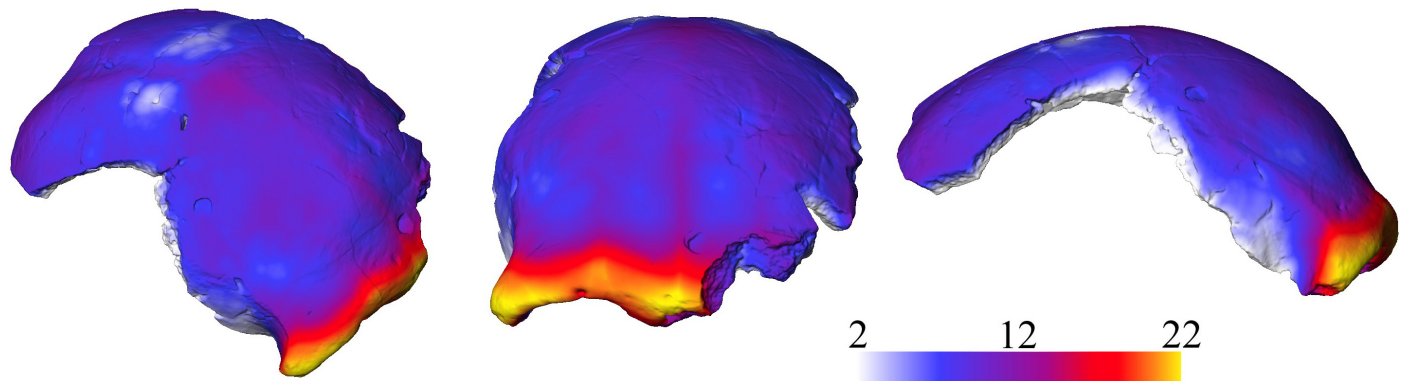


Figure 6. Heat map of cranial vault thickness generated from the micro-CT scan of the Florisbad calotte in 3/4 antero-superior, anterior, and right latera views. Note the overall symmetry of thickness across the entire calotte, and the moderate thickening around bregma (in the middle of the image, in purple). The apparent midline thickening of the frontal above the supraorbital torus is a reflection of the frontal crest (in the middle of the anterior view).

TABLE 2. CRANIAL VAULT THICKNESS AND INTERNAL BONE COMPOSITION MEASURED AT BREGMA, THE MID-FRONTAL POINT IN THE MID-SAGITTAL PLANE, AND THE POINT IN THE CENTER OF THE RIGHT PARIETAL.

Location	CVT	Internal table	Diploic layer	External table
Bregma	11.6	1.7	7.3	2.6
	<i>% of CVT</i>	<i>14</i>	<i>63</i>	<i>22</i>
Mid-Frontal MSP	11.3	1.3	8.5	1.5
	<i>% of CVT</i>	<i>12</i>	<i>75</i>	<i>13</i>
Mid-Parietal R	8.8	1.6	6.0	1.3
	<i>% of CVT</i>	<i>18</i>	<i>68</i>	<i>14</i>

The values are the absolute dimension in mm. The percentage contribution of each layer's thickness to total thickness at each point is indicated in italics.

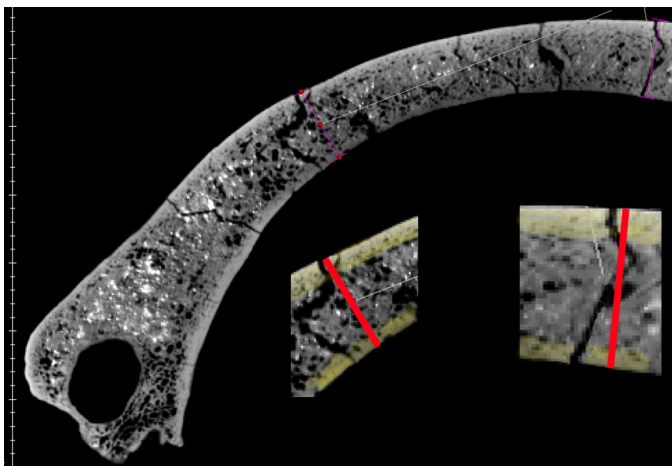


Figure 7. The midsagittal plane of the Florisbad calotte showing the positions at which thickness and bone structure were quantified in the middle of the frontal bone and at bregma. The zoomed areas show the extent of the internal and external tables (highlighted in yellow), which can be clearly delineated from the diploë. Note the inclusion of sediment (in white) in the diploë and the presence of cracks traversing the vault.

Diploic Channels

Most of the diploë have been infiltrated by sediment, which renders most of the diploic channels (DC) unidentifiable. However, several DC and emissary channel branches can be observed in the frontal and parietal bones (Figure 9). Incomplete DC branches that are distributed along the frontal crest and the right superior temporal line can be identified. The DC branch near the frontal crest is connected to a large foramen on the endocranial surface, which very likely forms a connection between the DC network and the superior sagittal sinus. The DCs near the superior temporal line

are adjacent to the meningeal vessels, possibly the orbital meningeal vessels (OMV) or middle meningeal vessels (MMV), and there are evident connections between them.

In the supraorbital torus, a DC branch courses mediolaterally over the orbit and connects to the periorbital or superficial temporal vessels through a large foramen on the external surface. Due to taphonomic damage, only a short channel is visible near the sinus that connects the diploë (Figure 10). Additionally, many emissary channels can be identified in the supraorbital torus, bridging the frontal sinus and the periorbital vessels (see Figure 10). The DC branches that are visible in the parietal bones are also incomplete. These branches are adjacent to the imprints of the posterior branch of the middle meningeal vasculature, but only a single foramen on the endocranial surface links a DC branch. The drainage pathways of other parietal DC branches are unclear due to their poor preservation.

Endocranial Morphology

The physical endocast of the Florisbad vault preserves the imprints of portions of the frontal and parietal lobes of the brain (Figure 11). Although it is affected by several cracks, the endocast, especially as reconstructed from the detailed micro-CT scans (Figure 12), retains a good deal of anatomical information beyond that described from the physical cast used by Dreyer and Kappers (1935) and from the laser surface scan employed by Bruner and Lombard (2020).

The imprints of the anterior meningeal vessels comprise several branches that course medially and posteriorly along the imprints of the middle and superior frontal convolutions on the right side. An imprint that could correspond to the sphenoparietal sinus is visible on the left frontal lobe, and a branch of the middle meningeal system is visible anteriorly to this. Three other branches run medio-posteriorly on the left frontal and parietal lobes. The

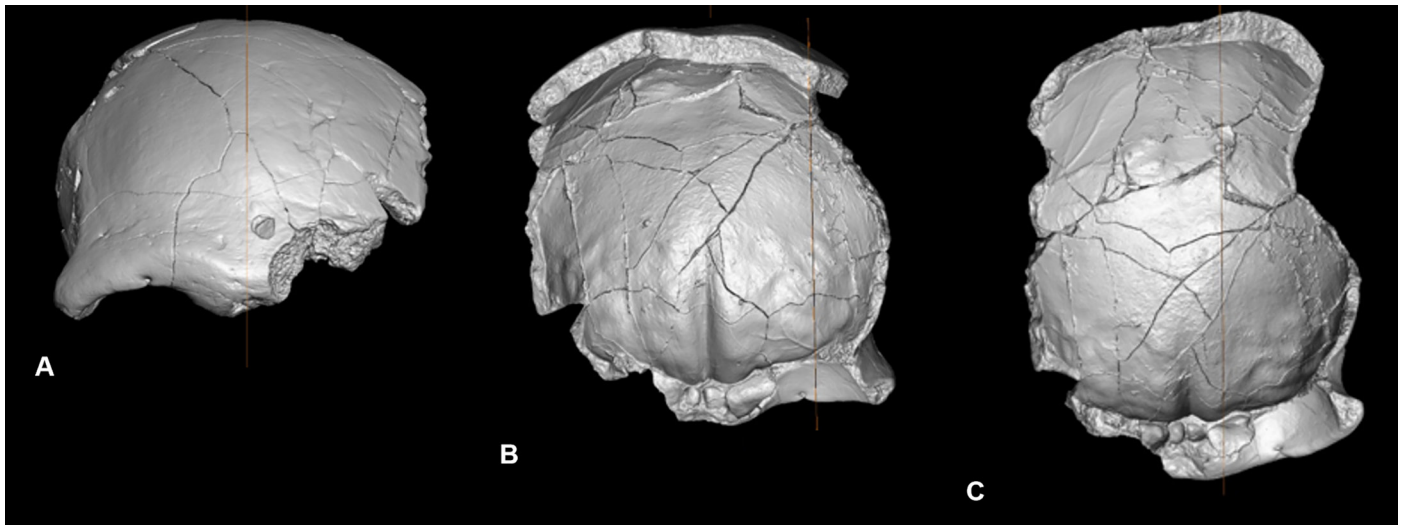


Figure 8. Location of the midsagittal plane (A) employed here to quantify bone thickness and its internal composition, and the locations of the two planes (B and C) used by Curnoe and Brink (2010: Figures 4B and 4C).

posterior extension of three meningeal vessels is visible on preserved part of the right parietal lobe although they do not reach the superior parietal lobule. The superior sagittal sinus is visible between the parietal lobes and several sizeable Pacchionian impressions are visible.

Concerning the imprints of the gyri and sulci, small parts of the inferior, medial and superior frontal sulci are visible in the anterior portions of the frontal lobes. Part of the central sulcus is observable in its uppermost extension on the left side.

Frontal Sinus Development

The right frontal sinus is nearly complete (Figure 13), although its inferomedial extent is missing. Only the superior and medial extensions of the left sinus are preserved as the roof of the left orbit is damaged. The right sinus is a large, globular cell that extends laterally to the level of the summit of the orbit and medially to the left of the median sagittal plane. Based on the preserved part of the left sinus, it is very likely that it was somewhat smaller than that on the right, with more restricted medial, posterior, and supero-inferior extensions. Although its other width dimensions cannot be measured directly, its probable size can be estimated based on its shape and by comparison with the sinus on the right side.

On the basis of the preserved parts of the frontal pneumatization, we measured its dimensions in 3D using the variables defined by Balzeau et al. (2022) (see Table 1 for the definitions of the various measurements, and Table 3 for the results). The anterior length of the right sinus (ALr 31.4mm), superior length (SLr 32.6mm), as well as the height (H 22.8mm) and the two dimensions that describe the antero-posterior extension of the sinuses, AP (21.4mm) and AP2 (21.0mm), could be measured without being compromised by the incomplete preservation of the left pneumatic space. Estimated dimensions are width (58.2mm), the anterior length of the left sinus, ALl (21.0mm) and the

superior length of the left sinus, SLl (18.6mm). These estimates were based on the preserved shape of the left sinus and the comparison with the shape and dimension of the right sinus, which is globally larger, providing an estimate of the maximum expansion of pneumatization.

The entire frontal sinus is estimated to have had a volume of approximately 9.7cm³ (mL) as determined by segmentation of the right sinus and extrapolation to the left.

COMPARISONS WITH OTHER PLEISTOCENE FOSSILS

The results of our analyses of cranial vault thickness, endocranial dimensions, and frontal sinus size invite comparison with published data on other Middle and Late Pleistocene *Homo* fossils and with recent human samples.

Cranial Vault Thickness

In terms of average CVT as measured along the parasagittal section across the frontal and parietal, the Florisbad cranium has a thinner vault than the other two Middle Pleistocene crania included in our dataset, Kabwe 1 and Petralona (Table 4). Topographic mapping (Figure 14) indicates that the thickest regions of the Florisbad calotte are located in the same areas as those in the Kabwe 1 cranium even if the former does not reach the same values of thickness. In Florisbad, the reddish hues that highlight the areas with thickness of over 17mm appear only locally along the frontal torus, with thickening also around the anterior border of the bregmatic region. In Kabwe 1, while the vault immediately behind the supraorbital torus is very thick, the median sagittal band tends to be thinner than the frontal and parietal bosses, although there is a small region of thicker bone at bregma, whereas the midline and especially the bregmatic regions are thicker in Florisbad (see Figure 14). The bregmatic region also shows thickening in Asian *H. erectus* crania (Balzeau 2013).

Thickness distribution across the vault in Florisbad

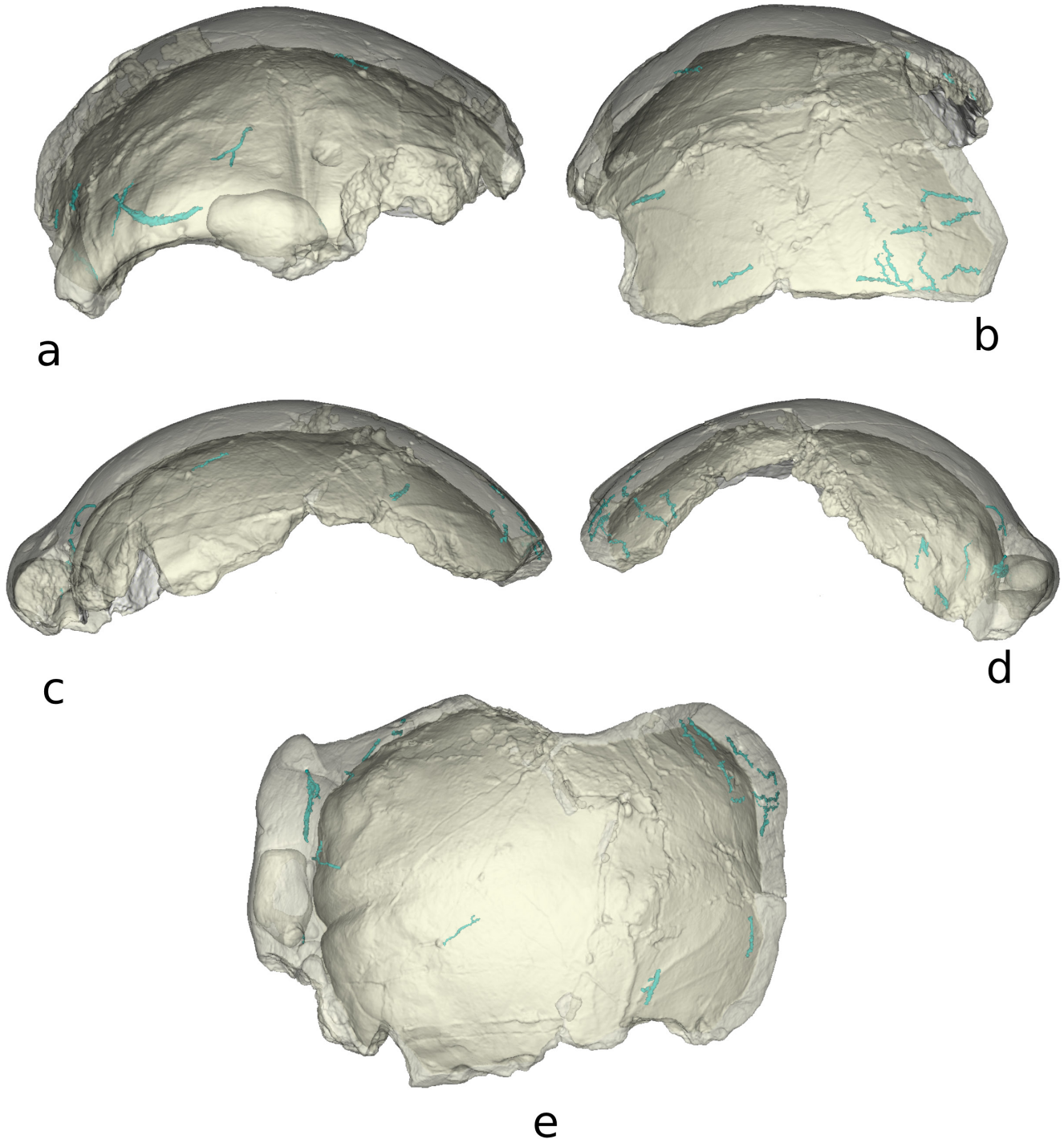


Figure 9. The diploic channels (in blue) in the translucent images of the Florisbad calotte, seen in a) anterior, b) posterior, c) left lateral, d) right lateral, and e) superior views.

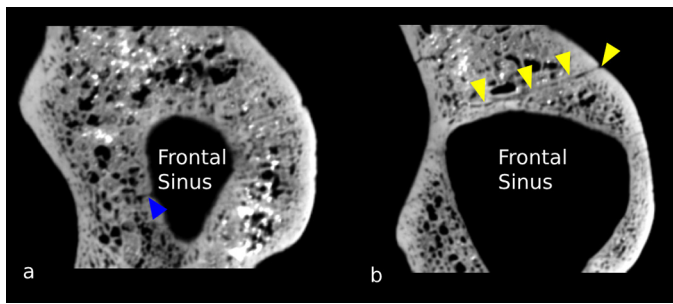


Figure 10. Micro-CT scans of two parasagittal sections through the supraorbital torus. The short channel (blue arrow in a) links the frontal sinus and the diploë. An emissary channel (yellow arrows in b) connects to the extracranial vascular network in the supraorbital torus.

does not follow the patterns for either *H. sapiens* or *H. neanderthalensis* (Balzeau 2013) (see Figure 14). In particular, there is no clear thinning along the midline of the frontal and parietal as is frequently observed in fossil *H. sapiens*. Rather, there is a thickening anteriorly to the bregma and thinning in the anterior part of the parietal bones. The medial aspects of the Florisbad parietals are relatively thick.

The mean CVT value obtained for Florisbad (8.6mm) is within the upper limits of the observed ranges for the *H. erectus* and fossil *H. sapiens* samples, and slightly exceeds the range observed for *H. neanderthalensis* and recent *H. sapiens* (see Table 4).



Figure 11. Anterior view of the hard copy plastic endocast of the Florisbad calotte produced directly from a silicon mold of the calotte by Ron Clarke. Note the depression of the midline superior sagittal sinus posterior to the impression of the frontal crest.

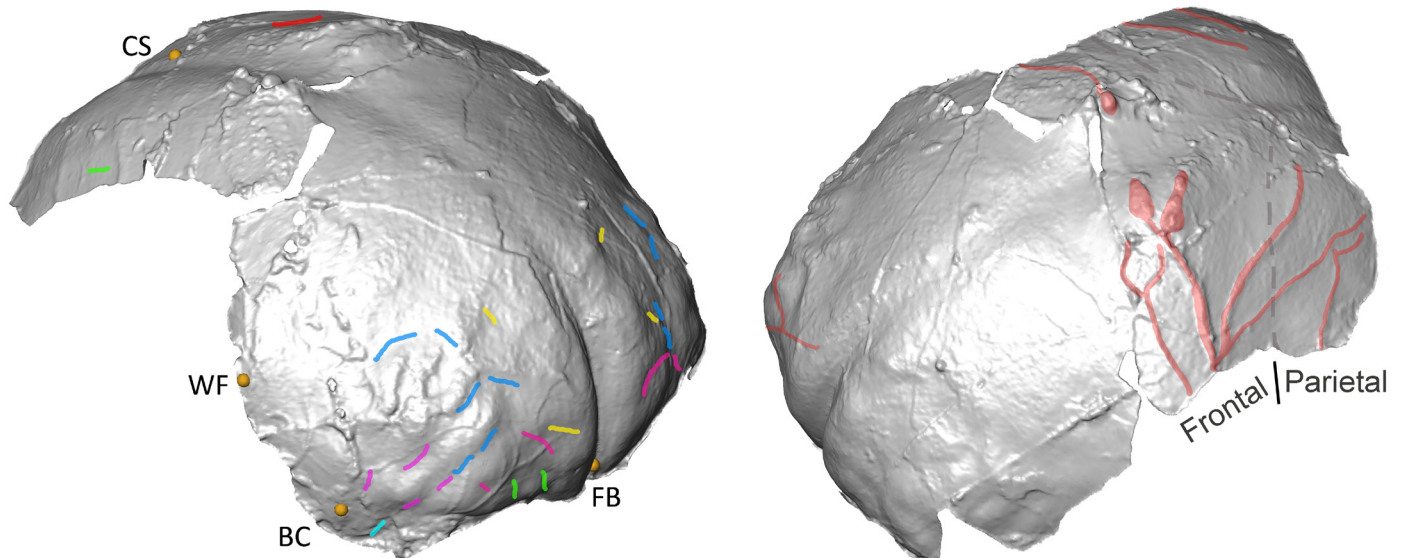


Figure 12. Three-quarter views of the virtual endocast of the Florisbad calotte showing the position of the landmarks (from left to right: intersection of the central sulci CS, maximum width of the frontal lobes WF, Broca's cap BC, frontal bec FB) used to measure several linear distances (frontal cord, width at the Broca's cap, maximal frontal width) and the visible brain sulci on the left (light green: orbital sulci; pink, blue, and yellow: frontal sulci; light blue: horizontal sulcus; green on the parietal lobe: intraparietal sulcus; red: central sulcus), and the meningeal system (in red) on the right, with a possible relief corresponding to the sphenoparietal sinus (the second imprints from the left that connects medially with two Pacchionian depressions), as well as the extension of the frontal and parietal lobes.



Figure 13. Anterior view of the Florisbad calotte shown in grey by transparency and the preserved frontal sinuses in black. The right sinus is nearly completely preserved, the left sinus is smaller and less well-preserved.

Finally, the arachnoid villi (Pacchionian) depressions in Florisbad, which are associated to reduced internal bone thickness, are distributed over a similar extended area over the medial and anterior part of the parietal as in Cro-Magnon 1. The sizes of the depressions in Florisbad are similar to those reported for Kabwe 1 and Cro-Magnon 1 (see Figure 14; see also Balzeau et al. 2013; 2017). The sizes of the arachnoid depressions fall comfortably within the range of variation of non-pathological samples of various hominin species (Holloway et al. 2003).

Diploic Channels

The diploic channels (DCs) may provide a taxonomic signal at some level, as revealed by studies that have shown that the DC networks of non-human primates are much less developed than those of hominins (Hershkovitz et al. 1999; Hui 2024). Anastomoses between the DCs and parietal foramina are frequent in non-human primates, most fossil hominins, and extant humans, while the absence of parietal foramina and their connections with DCs is spe-

TABLE 3. LINEAR DIMENSIONS (in mm) OF THE FRONTAL SINUS.

W	H	Alr	All	2AL	SLr	SLI	2SL	AP	AP2	2AP
58.2	22.8	31.4	21.0	52.4	32.6	18.6	51.2	21.4	21.0	42.4

For definitions of these variables, see Table 1. Values in italics are estimates.

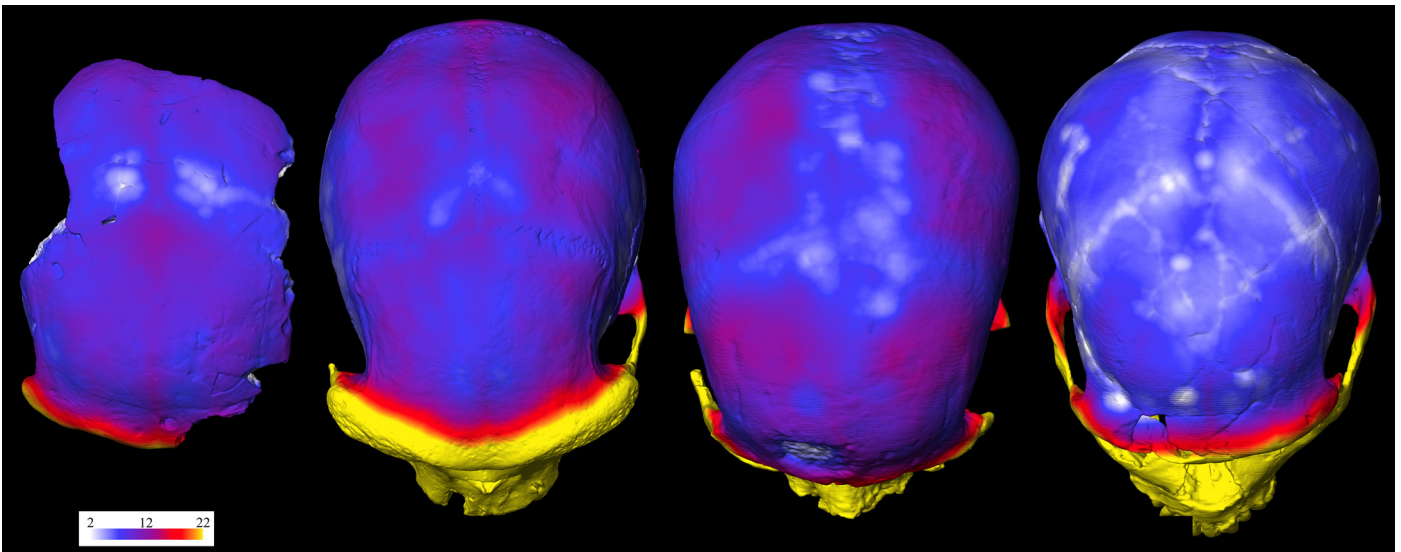


Figure 14. 3D topographic maps of the variation of total vault bone thickness rendered using a color chromatic scale (thickness increases from white to yellow, corresponding to a variation between 2mm and 22mm) in superior views for (from left to right) Florisbad, Kabwe 1 (*H. rhodesiensis*), Cro-Magnon 1 (*H. sapiens*), and La Ferrassie 1 (*H. neanderthalensis*).

TABLE 4. AVERAGE CVT VALUES (mm) FOR THE PARASAGITTAL SWATH ACROSS THE FRONTAL AND PARIETALS IN FLORISBAD AND IN PLEISTOCENE AND RECENT *HOMO* CRANIA.

Sample	n	Mean	SD	Obs. Range
Middle Pleistocene <i>Homo</i>				
Florisbad	1	8.6		
Kabwe 1	1	10.0		
Petralona	1	10.1		
<i>Homo erectus</i>	9	7.4	1.0	5.8–9.1
<i>Homo neanderthalensis</i>	7	6.3	0.9	4.5–7.4
Fossil <i>Homo sapiens</i>	23	7.7	1.2	5.8–10.2
Recent <i>Homo sapiens</i>	40	6.1	1.0	4.0–8.0

The comparative samples are the same as employed by Balzeau (2013). The *H. erectus* sample is comprised by: KNM-ER 3733, KNM-ER 3883, Sangiran 2, Ngawi 1, Ngandong 1, Ngandong 7, Ngandong 12, Sambungmacan 1, and Sambungmacan 3. The *H. neanderthalensis* sample is comprised by: La Chapelle-aux-Saints, La Ferrassie 1, Guattari, La Quina H5, Saccopastore 1, Spy 1, and Spy 2. The fossil *H. sapiens* sample is comprised by: Skhul V, Cro-Magnon 1, Cro-Magnon 2, Cro-Magnon 3, Mladeč 1, Pataud, Rochereil, Song Terus, Téviec 8, Téviec 9, Téviec 16 and North African Epi-Palaeolithic crania from Afalou Bou Rhummel (Afalou 2, 12, 13, 28, 30, 34) and Taforalt (Taforalt XI C1, XII C1, XV C2, XV C4, XV C5, XVII C1). The recent *H. sapiens* sample is comprised of 20 male and 20 female crania from Europe.

cific to *H. neanderthalensis* (Hui and Balzeau 2023; Hui et al. in press). Another feature of *H. neanderthalensis* is the isolation between the parietal DC and the transverse sinus, while these two vessels are usually anastomosed in other Hominidae species (Hui 2024). Moreover, anastomoses between DCs and the frontal sinus are consistently present in non-human primates and most hominin species. Still, this DC anastomosis with frontal sinuses is not regularly found in *H. sapiens* (Hui 2024). However, in the Florisbad cranium, these areas and structures with taxonomic significance were not well preserved. This hindered us from applying DCs in estimating the affinities of Florisbad.

Endocranial Dimensions

We were able to measure three linear distances on the Florisbad endocast. Comparison of the absolute values of the three linear distances assessed in Florisbad and in the comparative Pleistocene *Homo* fossils and recent humans (Table 5) confirms the large size of the Florisbad endocast. A PCA was computed on these linear dimensions. The three variables have positive loadings along PC1, which represents nearly 90% of the total variance (Figure 15). PC1 is therefore highly related to variations in global size of the analyzed specimens. The loadings of the three measurements are respectively 0.66 for FalCE, 0.44 for WBE, and 0.6 for MFWE along PC1. This component discriminates specimens of *Australopithecus africanus* and *H. habilis*, in the negative quadrant, from *H. erectus* in the middle and, in the positive quadrant, from large-brained *H. sapiens*. Florisbad

plots comfortably in the latter area. Florisbad is significantly larger than early hominins and it is larger also than *H. erectus* for the maximum width measured at the Broca's cap (see Table 5), as revealed by the adjusted z-scores. No discrimination between the different groups is apparent along PC2. The loadings of the three measurements are respectively -0.75 for FalCE, 0.36 for WBE, and 0.56 for MFWE along PC2.

With regard to the relative values of the endocast, those for Florisbad differ from recent *H. sapiens*, and approximate those of Kabwe 1 (Figure 16). This is due to a relatively restricted AP length of the frontal lobes compared to their width. In this PCA, the discrimination between the different groups is not very clear due to the small number of variables involved. PC1 represents 53.8% of the total variance; *Homo sapiens* specimens mostly occupy the negative area of the axis while the fossil groups tend to be in the positive area. The loadings of the three measurements are respectively -0.01 for FalCE, 0.68 for WBE, and 0.72 for MFWE along PC1 and 0.99 for FalCE, 0.06 for WBE, and -0.08 for MFWE along PC2.

The adjusted z-scores provide a direct comparison between Florisbad and the comparative samples (see Table 5). With regard to the relative dimensions, the frontal cord in Florisbad has lower values in comparison to all other samples, and the width at Broca's cap is significantly larger than in recent *H. sapiens*.

These analyses are, of course, limited by the restricted amount of information that we could quantify on the in-

TABLE 5. MEASUREMENTS* OF THE ENDOCAST OF FLORISBAD (in mm) (compared with Kabwe, Djebel Irhoud 1, LH 18, early hominins, *Homo erectus*, *H. neanderthalensis* and *H. sapiens*).

	FalCE	WBE	MFWE	FalCEr	WBEr	MFWEr
Florisbad	133.1	109.4	117.7	113.1	97.8	105.2
Kabwe	124.1	99.5	119.2	113.0	90.6	108.5
Djebel Irhoud 1	117.1	101.6	117.2	107.2	92.9	107.3
LH18	127.9	94.4	106.6	115.2	85.0	96.0
early hominins (n=7)						
Mean	93.2	75.7	83.6	116.8	95.0	104.8
SD	6.6	3.9	6.3	5.6	5.0	5.2
Max	105.2	80.6	94.8	126.0	103.2	113.5
Min	84.3	69.3	76.6	110.7	86.7	95.9
Azs	2.3	3.3	2.1	-0.3	0.2	0.0
<i>Homo erectus</i> (n=13)						
Mean	120,0	91.1	104.5	119.7	90.9	104.4
SD	10.6	7.2	6.5	5.4	3.9	4.1
Max	137.8	104.5	113,0	128.8	97.7	122.3
Min	102.8	82.3	94.1	108.6	83.1	97.2
Azs	0.5	1.1	0.9	-0.5	0.8	0.1
<i>Homo neanderthalensis</i> (n=8)						
Mean	129.0	102.3	116.6	115.8	91.7	104.6
SD	6.4	6.6	5.0	3.4	4.3	3.5
Max	137.7	111.3	122.2	121.8	100.5	112.1
Min	118.2	91.3	108.8	109.8	86.6	101.6
Azs	0.3	0.5	0.1	-0.4	0.6	0.1
<i>Homo sapiens</i> (recent n=35, fossil n=10)						
Mean	134.2	99.6	118.8	117.6	87.3	103.8
SD	6.7	6.4	9.2	4.7	4.3	5.7
Max	152.4	113.9	139.0	128,0	98.3	113.3
Min	122.3	85.2	102.4	109.8	78.4	92.3
Azs	-0.1	0.8	0.0	-0.5	1.2	0.1

*The frontal cord extends between the frontal bec and the junction of the central sulci (denoted FalCE), the width at the Broca's cap (denoted WBE), and the maximum width of the frontal lobes (denoted MFWE); see Figure 2. Relative dimensions are indicated by a r Azs scores: bold values indicate values of the analyzed specimen that is beyond 95% of the variation of the reference sample.

complete Florisbad endocast. Nevertheless, they are informative of the general shape of the preserved areas.

Frontal Sinus Size

The absolute volume estimated for the frontal pneumatization of Florisbad, which includes both the left and right sinuses, is compared to the values recorded for several

Middle Pleistocene *Homo* fossils and the means for samples of *H. erectus*, *H. neanderthalensis*, and recent sub-Saharan African populations in Table 6. At 9.70ml, the Florisbad sinus is notably smaller than those of Kabwe 1 and especially Petralona and Bodo. It is somewhat larger than the mean value of the *H. erectus* sample and only slightly smaller than the *H. neanderthalensis* sample mean, but it falls very

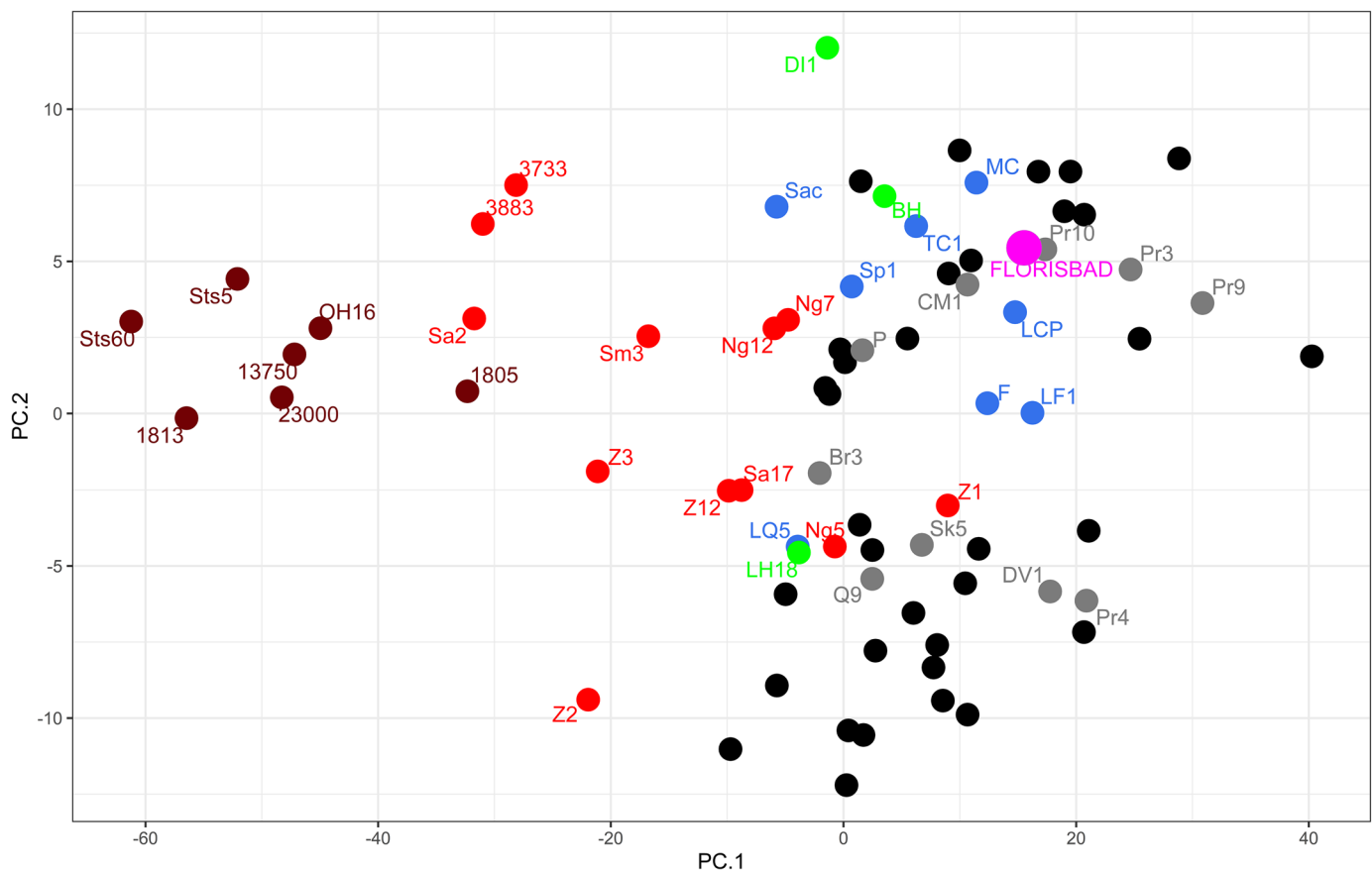


Figure 15. PCA of absolute measurements of endocranial dimensions (FalCE, WBE, and MFWE as visible on Figure 2; see also Table 5 for the detailed metric data). PC 1 represents 89.7% of the variance and PC2, 7.5%. Early hominins in dark red (Sts 5 and 60, KNM-ER 1813, 13750 and 23000, OH 16); *H. erectus* in red (KNM-ER 3733 and 3883, Z is used for Zhoukoudian 1, 2, 3, and 12, Sa for Sangiran 2 and 17, Sm3 for Sambungmacan 3, Ng for Ngandong 5, 7, 12); *H. neanderthalensis* in blue (F for Feldhofer, LCP for La Chapelle aux Saints, LF1 for La Ferrassie 1, LQ5 for La Quina H5, MC for Monte Circeo, Sac for Saccopastore, SP1 For Spy 1, TC for Tabun C1); fossil *H. sapiens* in grey (Br3 for Brno 3, CM1 for Cro-Magnon 1, DV1 for Dolni Vestonice, Q9 for Qafzeh 9, P for Abri Pataud, Pr for Predmosti 3, 4, 9, and 10, Sk5 for Skhul V); recent *H. sapiens* in black; specimens with a debated attribution (DI1 for Djebel Irhoud 1, BH for Broken Hill-Kabwe 1, and LH 18) in green; Florisbad in pink.

comfortably within the fiducial limits for both samples. Moreover, the Florisbad sinus volume exceeds the means of all five recent sub-Saharan African samples, although it is within 1 SD of the means of the South African sample reported by Greening et al. (2024) and the West African sample reported by Butaric et al. (2022). The Florisbad sinus volume is, however, significantly larger than the comparatively small mean volume reported for the South African Later Stone Age Khoe-San sample (Grine et al. 2024).

The linear dimensions for the frontal sinuses of Florisbad were projected into a linear discriminant analysis computed from the data compiled by Balzeau et al. (2022: S3). The groups in those analyses were early hominins, *H. erectus*, *Homo neanderthalensis*, and *H. sapiens*. Florisbad classifies as *H. erectus* with respect to the absolute dimensions and as *H. neanderthalensis* with respect to the relative dimensions for the frontal sinus. The percentages of correct classification are 79.6% for the absolute and 64.5% for the

relative dimensions (and respectively 79% and 62.5% with cross-validation). Such levels of correct classification are quite high despite the considerable variation in the shape and size of the frontal sinuses and are likely related to the fact that we have used large comparative samples. However, it shows that differences are indeed present between those groups. The calculated classifications for Florisbad, as *H. erectus* and *H. neanderthalensis*, are related to the globular sinuses that fill a large part of the medial part of the supraorbital torus. In those aspects, this specimen is different from the characteristics observed in *H. sapiens* (Balzeau et al. 2022).

DISCUSSION AND CONCLUSIONS

Our results do not support the presence of cranial vault asymmetry in Florisbad as suggested by Curnoe and Brink (2010). Rather, data from micro-CT scans confirm that the internal composition and distribution of bone thickness in

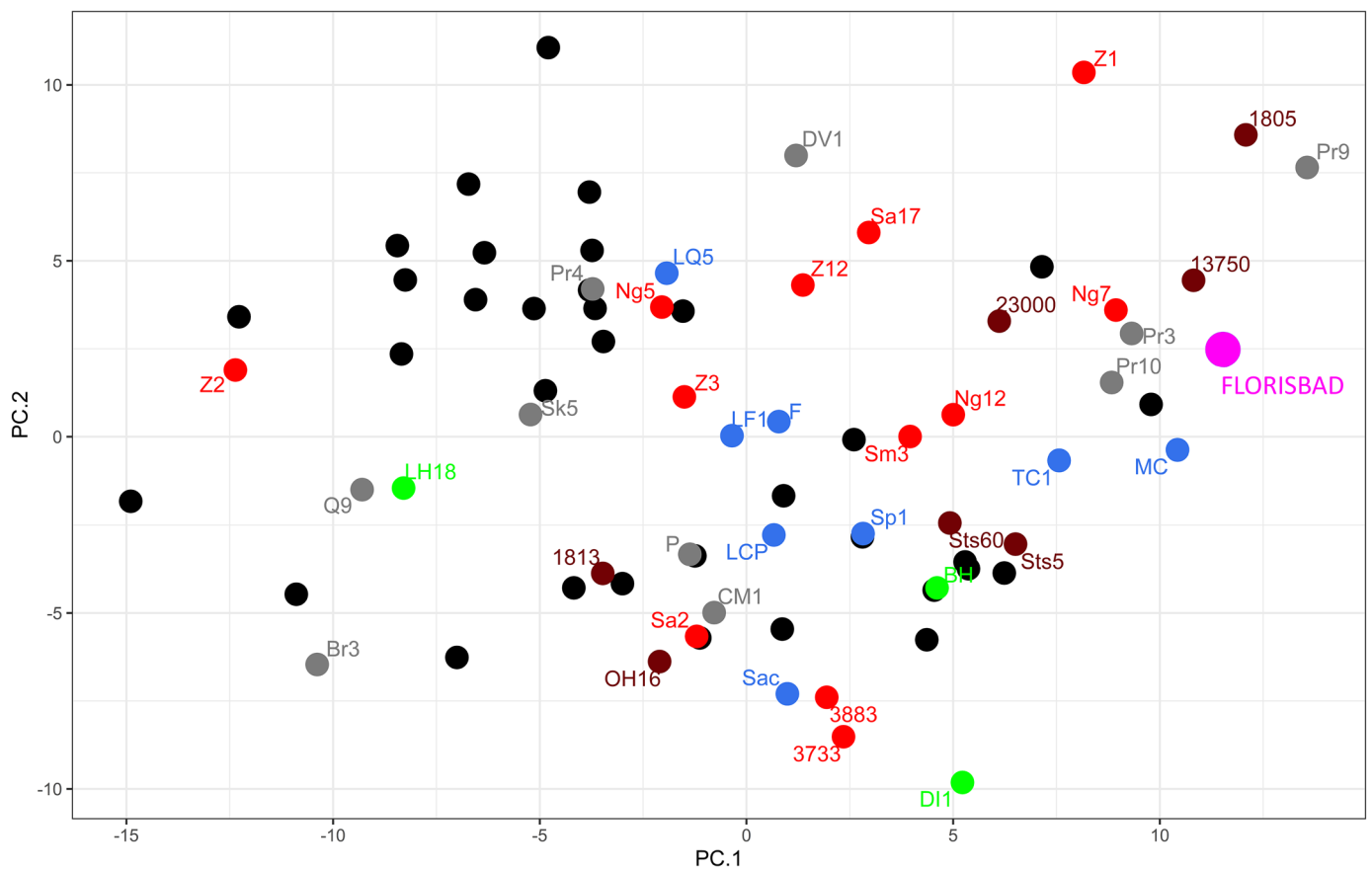


Figure 16. PCA of relative (size-adjusted, i.e., $FalCE$, WBE , and $MFWE$ divided by the respective endocranial volume ($(xi/(3\sqrt{EVi}) * 100)$) measurements of endocranial dimensions (see Table 5 for the metric data). PC 1 represents 53.8% of the variance and PC2, 29.9%. Early hominins in dark red, *Homo erectus* in red, *Homo neanderthalensis* in blue, fossil *Homo sapiens* in grey, recent *Homo sapiens* in black, specimens with a debated attribution (DI1 for Djebel Irhoud 1, BH for Broken Hill-Kabwe 1 and LH 18) in green, and Florisbad in pink (abbreviations are the same as in Figure 15).

this calotte correspond to those observed in other Middle and Late Pleistocene hominin specimens with no pathological alteration.

The vault in this specimen is not particularly thick when compared to other fossils from various hominin species (Balzeau 2013; Balzeau et al. 2017; Copes and Kimbel 2016), including *H. sapiens* (Marsh 2013) contrary to the suggestion of Curnoe and Brink (2010). The distribution of CVT is seen as normal when it is compared to other fossil hominins and is not asymmetric. In addition, the internal composition of the vault bone is not affected by any pathology and falls within the variation observed in samples of *H. erectus* (Balzeau 2006) and recent *H. sapiens* (Copes 2016). The proportions measured here for Florisbad are well within the range of variation observed among our comparative samples, indicating the lack of a pathological condition. In fact, clinical indicators of pathology in the proportion of the diploë relative to the tabular tables in living humans (e.g., Stuart-Macadam 1987) appear not to be appropriate for interpretive inferences relating to fossil hominin crania whose CVT is larger than that of living people.

Concerning the Pacchonian depressions that are visible on the endocranial surface of the calotte, they are not particularly large compared to those seen in many other fossil hominins, including Kabwe 1.

Thus, the features listed by Curnoe and Brink (2010) to suggest a pathological condition for the Florisbad cranium are not confirmed by the present study. Part of the discrepancy is likely due to the fact that they employed imaging technology that was inadequate for the task. In addition, their use of unique parasagittal slices is methodologically problematic and results in erroneous observations. The same limitation has been reported in previous descriptions of possible pathological traits in *H. floresiensis* by Jacob et al. (2006) and Henneberg et al. (2014), which have been corrected by Balzeau and Charlier (2016) with more precise imaging datasets. While researchers have to employ all data available to them, they should carefully consider the methodological limitations of such information in order to avoid overinterpretation.

This study of the Florisbad cranium has served to expand our knowledge of the anatomy of the specimen, in-

TABLE 6. ABSOLUTE FRONTAL SINUS VOLUMES (ml) RECORDED FOR FLORISBAD, PLEISTOCENE *HOMO* FOSSILS AND COMBINED SEX RECENT INDIGENOUS SUB-SAHARAN AFRICAN HUMAN POPULATIONS SAMPLES (direct volumetric measurement from segmented CT scans).

Population	n	volume	SD	Reference
Florisbad	1	9.70		This study
Kabwe 1	1	34.90		Balzeau et al. (2022: S3)
Petralona 1	1	84.37		Balzeau et al. (2022: S3)
Bodo 1	1	64.45		Balzeau et al. (2022: S3)
<i>Homo erectus</i>	12	7.80	4.01	Balzeau et al. (2022: S3)
<i>Homo neanderthalensis</i>	12	9.81	3.98	Balzeau et al. (2022: S3)
Sub-Saharan <i>H. sapiens</i>				
LSA Khoe-San	102	2.92	1.75	Grine et al. (2024)
South African	330	7.65	--	Rennie et al. (2017)
South African	150	8.58	7.40	Greening et al. (2024)
West African	27	6.09	3.39	Butaric et al. (2022)
West African	13	5.12	2.22	Buck et al. (2019)

cluding previously undocumented features. In this context, we observe that several anatomical traits differ from the condition observed in recent *H. sapiens*. The vault is relatively thick, with no thinning in the medial extension of the frontal and parietal lobes. The pattern of distribution of CVT is similar to that of Kabwe 1 (Balzeau et al. 2017) and differs from that in both *H. neanderthalensis* and *H. sapiens* (Balzeau et al. 2013). On the endocast, the middle meningeal vascular system is not well-developed. Endocranial dimensions are large and illustrate a lateral expansion of the frontal lobes relative to their lengths. Overall, the shape of the frontal lobes is more similar to that seen in Kabwe 1 and *H. neanderthalensis* than to what is characteristic of *H. sapiens* (Balzeau et al. 2013).

The diploic venous system is important to cranial blood circulation, as it facilitates the exchange between extra- and intra-cranial blood. The specific differences between hominins and non-human great apes (Hui and Balzeau 2023, 2024) suggest that the diploic venous system has potential application in taxonomic and phylogenetic discussions, especially in distinguishing between *H. neanderthalensis* and *H. sapiens*. The system of diploic channels, even if not fully preserved in Florisbad, appears to have been less expanded than in *H. sapiens* (Hui and Balzeau 2023).

Finally, the globular frontal sinus in Florisbad fills the medial region of the frontal torus. In this regard, the specimen more closely resembles the sinuses observed in *H. erectus* and *H. neanderthalensis*. The volume of the frontal sinus in Florisbad is within the fiducial limits for *H. erectus*, *H. neanderthalensis*, and most recent sub-Saharan African population samples. It is notably larger than the average

volume recorded for South African Later Stone Age (Holocene) Khoe-San.

In terms of its cranial bone distribution and endocranial proportions, Florisbad resembles the Middle Pleistocene cranium from Kabwe. Florisbad, however, does not share the exceptionally large frontal sinuses seen in this specimen, which are evident also in the Bodo and Petralona crania. Further comparison of the internal anatomical features described here may help in the future to clarify the polarity of these traits, and aid in the interpretation of various Pleistocene fossils.

ENDNOTES

¹The base of the Middle Pleistocene is 774 ka BP and the base of the Late Pleistocene is 129 ka BP (Head et al. 2021).

ACKNOWLEDGEMENTS

This study was funded by the French National Research Agency (ANR-20-CE27-0009) and the China Scholarship Council (JH), and by Stony Brook University (FEG). We are grateful to the National Museum, Bloemfontein, South Africa, for having granted permission to FEG and SH to micro-CT scan the Florisbad cranium. We thank Ron Clarke for discussions relating to the preservation and morphology of the Florisbad fossil. We thank the editor and the three anonymous reviewers who provided useful comments that served to strengthen this paper.

DATA AVAILABILITY STATEMENT

The Florisbad cranium is curated by the National Museum, Bloemfontein, South Africa. The measurements for Flo-

risbad have been provided in this article. The data for the comparative samples are available in the various papers we have published on the different anatomical areas studied here.

The authors declare no conflict of interest



This work is distributed under the terms of a [Creative Commons Attribution-NonCommercial 4.0 Unported License](https://creativecommons.org/licenses/by-nc/4.0/).

REFERENCES

- Bae, C.J., Wu, X., 2024. Making sense of eastern Asian Late Quaternary hominin variability. *Nat. Commun.* 15, 9479.
- Balzeau, A., 2006. Are thickened cranial bones and equal participation of the three structural bone layers autapomorphic traits of *Homo erectus*? *Bull. Mém. Soc. Anthropol. Paris* 18, 145–163.
- Balzeau, A., 2007. Variation and characteristics of the cranial vault thickness in Krapina and Western European Neandertals. *Period. Biol.* 109, 369–377.
- Balzeau, A., 2013. Thickened cranial vault and parasagittal keeling, correlated traits and autapomorphies of *Homo erectus*? *J. Hum. Evol.* 64, 631–644.
- Balzeau, A., Charlier, P., 2016. What do cranial bones of LB1 tell us about *Homo floresiensis*? *J. Hum. Evol.* 93, 12–24.
- Balzeau, A., Buck, L.T., Albessard, L., Becam, G., Grimaud-Hervé, D., Rae, T.C., Stringer, C.B., 2017. The internal cranial anatomy of the Middle Pleistocene Broken Hill 1 cranium. *PaleoAnthropology* 2017, 107–138.
- Balzeau, A., Albessard-Ball, L., Kubicka, A.M., Noûs, C., Buck, L.T., 2021. Frontal sinus variation in extant species of the genera *Pan*, *Gorilla* and *Homo*. *Bull. Mém. Soc. Anthropol. Paris* 33, 27–52.
- Balzeau, A., Albessard-Ball, L., Kubicka, A.M., Beaudet, A., Santos, E., Bienvenu, T., Arsuaga, J.L., Asfaw, B., Berger, L., Bermúdez de Castro, J.M., Carlson, K., Clarke, R.J., Daura, J., Filippo, A., Gorgoulis, V.G., Grine, F.E., Harvati, K., Hawks, J., Herries, A., Hublin, J.J., Hui, J., Ives, R., Joordens, J.C.A., Kaifu, Y., Kouloukoussa, M., Lordkipanidze, D., Margvelashvili, A., Martin, J., Martínón-Torres, M., May, H., Mounier, A., Noûs, C., Rae, T., Röding, C., Sanz, M., Semal, P., Skinner, M., Stratford, D., Stringer, C., Suwa, G., Tawane, M., Temming, H., Tskoukala, E., White, T., Zilhao, J., Zipfel, B., Buck, L., 2022. Frontal sinuses and human evolution. *Sci. Adv.* 8, eabp9767.
- Bassinot, F. C., Labeyrie, L.D., Vincent, E., Quidelleur, X., Shackleton, N.J., Lancelot, Y., 1994. The astronomical theory of climate and the age of the Brunhes-Matuyama magnetic reversal. *Earth Planet. Sci. Lett.* 126, 91–108.
- Berger, L.R., Hawks, J., 2023. Revisiting the age of the Florisbad hominin material. *Homo* 74, 55–60.
- Bräuer, G., 2008. The origin of modern anatomy: by speciation or intraspecific evolution? *Evol. Anthropol.* 17, 22–37.
- Bräuer, G., Rimbach, K.W., 1990. Late archaic and modern *Homo sapiens* from Europe, Africa, and Southwest Asia: craniometric comparisons and phylogenetic implications. *J. Hum. Evol.* 19, 789–807.
- Bräuer, G., Groden, C., Delling, G., Kupczik, K., Mbua, E., Schultz, M., 2003. Pathological alterations in the archaic *Homo sapiens* cranium from Eliye Springs, Kenya. *Am. J. Phys. Anthropol.* 120, 200–204.
- Broom, R., 1913. Man contemporaneous with extinct animals in South Africa. *Ann. S. Afr. Mus.* 12, 13–16.
- Brothwell, D.R., 1974. The Upper Pleistocene Singa skull: a problem in palaeontological interpretation. In: Bernhard, W., Kalndler, A. (Eds.), *Bevölkerungsbiologie*. Gustav Fischer, Stuttgart, pp. 534–545.
- Bruner, E., Lombard, M., 2020. The skull from Florisbad: a paleoneurological report. *J. Anthropol. Sci.* 98, 89–97.
- Bruner, E., Athreya, S., de la Cuétara, J.M., Marks, T., 2013. Geometric variation of the frontal squama in the genus *Homo*: frontal bulging and the origin of modern human morphology. *Am. J. Phys. Anthropol.* 150, 313–323.
- Buck, L.T., Stringer, C.B., MacLarnon, A.M., Rae, T.C., 2019. Variation in paranasal pneumatization between Mid-Late Pleistocene hominins. *Bull. Mém. Soc. Anthropol. Paris* 31, 14–33.
- Butaric, L.N., Buck, L.T., Balzeau, A., du Plessis, A., Grine, F.E., 2022. The paranasal sinuses of the Hofmeyr cranium. In: Grine, F.E. (Ed.), *Hofmeyr. A Late Pleistocene Human Skull from South Africa*. Springer, Chaim Switzerland, pp. 179–211.
- Cassel, J. Harris, A.C., Harris, D.F., 1942. A preliminary comparative study of some Bushman and Strandloper cranial series. *S. Afr. J. Sci.* 39, 235–246.
- Chan, E.K., Hardie, R.A., Petersen, D.C., Beeson, K., Bornman, R.M., Smith, A.B., Hayes, V.M., 2015. Revised timeline and distribution of the earliest diverged human maternal lineages in southern Africa. *PLoS One* 10, e0121223.
- Clarke, R.J., 1985. A new reconstruction of the Florisbad cranium with notes on the site. In: Delson, E. (Ed.), *Ancestors: The Hard Evidence*. Alan R. Liss, New York, pp. 301–305.
- Cole, G., Waldron, T., 2019. Cribra orbitalia: dissecting an ill-defined phenomenon. *Int. J. Osteoarchaeol.* 29, 613–621.
- Copes, L.E., 2016. Cranial vault thickness in non-human primates: allometric and geometric analyses of the vault and its component layers. *J. Hum. Evol.* 101, 90–100.
- Copes, L.E., Kimbel, W.H., 2016. Cranial vault thickness in primates: *Homo erectus* does not have uniquely thick vault bones. *J. Hum. Evol.* 90, 120–134.
- Copes, L.E., Schutz, H., Dlugozs, E.M., Judex, S., Garland, T., 2018. Locomotor activity, growth hormones, and systemic robusticity: an investigation of cranial vault thickness in mouse lines bred for high endurance running. *Am. J. Phys. Anthropol.* 166, 442–458.
- Curnoe, D., Brink, J., 2010. Evidence of pathological conditions in the Florisbad cranium. *J. Hum. Evol.* 59, 504–513.

- de Villiers, H., 1968. The Skull of the South African Negro: A Biometrical and Morphological Study. Witwatersrand University Press, Johannesburg.
- Détroit, F., Mijares, A.S., Corny, J., Daver, G., Zanolli, C., Dizon, E., Robles, E., Grün, R., Piper, P.J., 2019. A new species of *Homo* from the Late Pleistocene of the Philippines. *Nature* 568, 181–186.
- Dreyer, T.F., 1938. The archaeology of the Florisbad deposits. *Archeolog. Navors. Nasionale Mus. Bloemfontein* 81, 65–77.
- Dreyer, T.F., 1947. Further observations on the Florisbad skull. *Soolog. Navors. Nasionale Mus. Bloemfontein* 151, 183–190.
- Dreyer, T.F., Kappers, C.U.A., 1935. A human skull from Florisbad, Orange Free State, with a note on the endocranial cast. *Koninkl. Akad. Wetenschap., Afdeel. Natuurkunde* 38, 119–128.
- du Plessis, A., le Roux, S.G., Guelpa, A., 2016. The CT Scanner Facility at Stellenbosch University: an open access X-ray computed tomography laboratory. *Nucl. Instrum. Methods Phys. Res. B* 384, 42–49.
- Galloway, A., 1936. Some prehistoric skeletal remains from the Natal coast. *Trans. R. Soc. S. Afr.* 23, 277–295.
- Galloway, A., 1937. The nature and status of the Florisbad skull as revealed by its nonmetrical features. *Am. J. Phys. Anthropol.* 23, 1–17.
- Galway-Witham, J., Stringer, C., 2018. How did *Homo sapiens* evolve? *Science* 360, 1296–1298.
- Greening, V.A., Hernandez, E., Mongle, C.S., Billings, B.K., Mngomezulu, V., Wallace, I.J., Grine, F.E., 2024. Variation, sexual dimorphism, and enlargement of the frontal sinus with age in adult South Africans. *Am. J. Biol. Anthropol.* 2024, e24899. <https://doi.org/10.1002/ajpa.24899>
- Grine, F.E., Holt, S., Brink, J.S., du Plessis, A., 2019. Enamel pearls: their occurrence in recent human populations and earliest manifestation in the modern human lineage. *Arch. Oral Biol.* 101, 147–155.
- Grine, F.E., Post, N.W., Greening, V., Crevecoeur, I., Billings, B.K., Meyer, A., Holt, S., Black, W., Morris, A.G., Veeramah, K.R., Mongle, C.S., 2024. Frontal sinus size in South African Later Stone Age Holocene Khoe-San. *Anat. Rec.* 2024, 1–26.
- Grobbelaar, C.S., Goodwin, A.J.H., 1952. Report on the skeletons and implements in association with them from a cave near Bredasdorp, Cape Province. *S. Afr. Archaeol. Bull.* 7, 95–107.
- Gronau, I., Hubisz, M.J., Gulko, B., Danko, C.G., Siepel, A., 2011. Bayesian inference of ancient human demography from individual genome sequences. *Nat. Genet.* 43, 1031–1034.
- Grün, R., 2006. Direct dating of human fossils. *Am. J. Phys. Anthropol.* 131, 2–48.
- Grün, R., Stringer, C., 2023. Direct dating of human fossils and the ever-changing story of human evolution. *Quatern. Sci. Rev.* 322, 108379.
- Grün, R., Brink, J.S., Spooner, N.A., Taylor, L., Stringer, C.B., Franciscus, R.G., Murray, A.S., 1996. Direct dating of Florisbad hominid. *Nature* 382, 500–501.
- Habgood, P., 1989. An examination of regional features on Middle and early Late Pleistocene sub-Saharan African hominids. *S. Afr. Archaeol. Bull.* 44, 17–22.
- Hautavoine, H., Arnaud, J., Balzeau, A., Mounier, A., 2024. Quantifying hominin morphological diversity at the end of the middle Pleistocene: implications for the origin of *Homo sapiens*. *Am. J. Biol. Anthropol.* 184, e24915.
- Henn, B.M., Steele, T.E., Weaver, T.D., 2018. Clarifying distinct models of modern human origins in Africa. *Curr. Opin. Genet. Devel.* 53, 148–156.
- Henneberg, M., Eckhardt, R.B., Chavanes, S., Hsü, K.J., 2014. Evolved developmental homeostasis disturbed in LB1 from Flores, Indonesia, denotes Down syndrome and not diagnostic traits of the invalid species *Homo floresiensis*. *Proc. Nat. Acad. Sci. USA* 114, 11967–11972.
- Hershkovitz, I., Greenwald, C., Rothschild, B. M., Latimer, B., Dutour, O., Jellema, L. M., Wish-Baratz, S., Pap, I., Leonetti, G., 1999. The elusive diploic veins: anthropological and anatomical perspective. *Am. J. Phys. Anthropol.* 108(3), 345–358.
- Hoffman, A.C., 1955. Important contributions of the Orange Free State to our knowledge of primitive man. *S. Afr. J. Sci.* 51, 163–168.
- Holloway, R.L., Broadfield, D.C., Yuan, M.S., Schwartz, J.H., Tattersall, I. (Eds.). 2004. The Human Fossil Record, Volume 3, Brain Endocasts—The Paleoneurological Evidence. Wiley-Liss, Hoboken, NJ.
- Hublin, J.J., Ben-Ncer, A., Bailey, S.E., Freidline, S.E., Neubauer, S., Skinner, M.M., Bergmann, I., Le Cabec, A., Benazzi, S., Harvati, K., Gunz, P., 2017. New fossils from Jebel Irhoud, Morocco and the pan-African origin of *Homo sapiens*. *Nature* 546, 289–292.
- Hui, J., 2024. Comparative anatomy of the diploic vessels in hominids: implications for the evolutionary history of human cranial blood circulation. Ph.D. Dissertation. Sorbonne University.
- Hui, J., Balzeau, A., 2023. The diploic venous system in *Homo neanderthalensis* and fossil *Homo sapiens*: a study using high-resolution computed tomography. *Am. J. Biol. Anthropol.* 182, 412–427.
- Hui, J., Balzeau, A., 2024. Investigating the relationship between cranial bone thickness and diploic channels: a first comparison between fossil *Homo sapiens* and *Homo neanderthalensis*. *Anat. Rec.* 307, 2036–2046.
- Hui, J., Wu, X., Balzeau, A., 2025. Reappraisal of the morphological affinities of the Maba 1 cranium: new evidence from internal cranial anatomy. *Am. J. Biol. Anthropol.* 187, e70064.
- Hurst, S.D., Holloway, R.L., Balzeau, A., Garvin, H.M., Vanti, W.B., Berger, L.R., Hawks, J., 2024. The endocast morphology of LES1, *Homo naledi*. *Am. J. Biol. Anthropol.* 2024, e24983.
- Imbrie, J., Hays, J.D., Martinson, D.G., McIntyre, A., Mix, A.C., Morley, J.J., Pisias, N.G., Prell, W.L., Shackleton, N.J., 1984. The orbital theory of Pleistocene climate: support from a revised chronology of the marine $\delta^{18}\text{O}$ record. In: Berger, A. (Ed.), *Milankovitch and Climate*,

- Part 1. D. Reidel, Hingham, MA, pp. 269–305.
- Jacob, T., Indriati, E., Soejono, R.P., Hsu, K., Frayer, D.W., Eckhardt, R.B., Kuperavage, A.J., Thorne, A., 2006. Pygmoid Australomelanesian *Homo sapiens* skeletal remains from Liang Bua: population affinities and pathological abnormalities. *Proc. Nat. Acad. Sci. USA* 103, 13421–13426.
- Kaifu, Y., Kurniawan, I., Mizushima, S., Sawada, S., Lague, M., Setiawan, R., Sutisna, I., Wibowo, U.P., Suwa, G., Kono, R.T., Sasaki, T.; Brumm, A., van den Bergh, G.D., 2024. Early evolution of small body size in *Homo floresiensis*. *Nat. Commun.* 15, 6381.
- Kohler, W.L., 1942. A survey of human skulls exhumed in the vicinity of Port Elizabeth. *S. Afr. J. Sci.* 39, 227–234.
- Kuman, K., Clarke, R.J., 1986. Florisbad - new investigations at a Middle Stone Age hominid site in South Africa. *Geoarchaeology* 1, 103–125.
- Kuman, K., Inbar, M., Clarke, R.J., 1999. Palaeoenvironments and cultural sequence of the Florisbad Middle Stone Age hominid site, South Africa. *J. Archaeol. Sci.* 26, 1409–1425.
- Kuman, K., 2023. Florisbad, South Africa. In: Beyin, A., Wright, D.K., Wilkins, J., Olszewski, D.I. (Eds.) *Handbook of Pleistocene Archaeology of Africa*. Springer, Cham, pp. 1451–1467.
- Labra, N., Mounier A., Leprince, Y., Rivière, D., Didier, M., Bardinet, E., Santin, M.D., Mangin, J.F., Filippo A., Albessard-Ball, L., Beudet, A., Broadfield, D., Bruner, E., Carlson, K.J., Cofran, Z., Falk, D., Gilissen, E., Gómez-Robles, A., Neubauer, S., Pearson, A., Röding, C., Zhang, Y., Balzeau, A., 2024. What do brain endocasts tell us? A comparative analysis of the accuracy of sulcal identification by experts and perspectives in palaeoanthropology. *J. Anat.* 244, 274–296.
- Laing, G.D., 1929. A final report on the Strandlooper skulls found at Zitzikama. *S. Afr. J. Sci.* 26, 575–601.
- Lisiecki, L.E., Raymo, M.E., 2005. A Plio-Pleistocene stack of 57 globally distributed benthic $\delta^{18}\text{O}$ records. *Paleoceanography* 20, PA2007.
- Mafessoni, F., Prüfer, K., 2017. Better support for a small effective population size of Neandertals and a long shared history of Neandertals and Denisovans. *Proc. Nat. Acad. Sci. USA*, 114, e10256.
- Mallick, S., Li, H., Lipson, M., Mathieson, I., Gymrek, M., Racimo, F., Zhao, M., Chennagiri, N., Nordenfelt, S., Tandon, A., Skoglund, P., 2016. The Simons genome diversity project: 300 genomes from 142 diverse populations. *Nature* 538, 201–206.
- McBrearty, S., Brooks, A.S., 2000. The revolution that wasn't: a new interpretation of the origin of modern human behavior. *J. Hum. Evol.* 39, 453–563.
- Mounier, A., Lahr, M.M., 2019. Deciphering African late middle Pleistocene hominin diversity and the origin of our species. *Nat. Commun.* 10, 3406.
- Meiring, A.J.D., 1956. The macrolithic culture of Florisbad. *Navors. Nasionale Mus.* 1, 205–237.
- Meneganzin, A., Pievani, T., Manzi, G., 2022. Pan-Africanism vs. single-origin of *Homo sapiens*: putting the debate in the light of evolutionary biology. *Evol. Anthropol.* 31, 199–212.
- Ni, X., Ji, Q., Wu, W., Shao, Q., Ji, Y., Zhang, C., Liang, L., Ge, J., Guo, Z., Li, J., Li, Q., Grün, R., Stringer, C., 2021. Massive cranium from Harbin in northeastern China establishes a new Middle Pleistocene human lineage. *Innovation (Camb)*. 28 2(3), 100130.
- Pantoja-Pérez, A., Arsuaga, J.L., 2024. The cranium I: neurocranium. *Anat. Rec.* 307, 2278–2324.
- Pearson, O.M., 2013. Africa: the cradle of modern people. In: Smith, F.H., Ahern, J.C.M. (Eds.), *The Origins of Modern Humans: Biology Reconsidered*, 2nd Edition. New York, Wiley, New York, pp. 1–43.
- Petr, M., Hajdinjak, M., Fu, Q., Essel, E., Rougier, H., Crevecoeur, I., Semal, P., Golovanova, L.V., Doronichev, V.B., Lalueza-Fox, C., de la Rasilla, M., Rosas, A., Shunkov, M.V., Kozlikin, M.B., Derevianko, A.P., Vernot, B., Meyer, M., Kelso, J., 2020. The evolutionary history of Neandertal and Denisovan Y chromosomes. *Science* 369, 1653–1656.
- Pinder, R.C., 2021. Using multiple luminescence chronometers to establish the chronology of the Middle Stone Age site of Florisbad, South Africa. Ph.D. Dissertation. Prifysgol Aberystwyth University.
- Protsch, R., 1975. The absolute dating of Upper Pleistocene sub-Saharan fossil hominids and their place in human evolution. *J. Hum. Evol.* 4, 297–322.
- Prüfer, K., Racimo, F., Patterson, N., Jay, F., Sankararaman, S., Sawyer, S., Heinze, A., Renaud, G., Sudmant, P.H., de Filippo, C., Li, H., Mallick, S., Dannemann, M., Fu, Q., Kircher, M., Kuhlwilm, M., Lachmann, M., Meyer, M., Ongyerth, M., Siebauer, M., Theunert, C., Tandon, A., Moorjani, P., Pickrell, J., Mullikin, J.C., Vohr, S.H., Green, R.E., Hellmann, I., Johnson, P.L.F., Blanche, H., Cann, H., Kitzman, J.O., Shendure, J., Eichler, E.E., Lein, E.S., Bakken, T.E., Golovanova, L.V., Doronichev, V.B., Shunkov, M.V., Derevianko, A.P., Viola, B., Slatkin, M., Reich, D., Kelso, J., Pääbo, S., 2014. The complete genome sequence of a Neanderthal from the Altai Mountains. *Nature* 505, 43–49.
- Prüfer, K., De Filippo, C., Grote, S., Mafessoni, F., Korlević, P., Hajdinjak, M., Vernot, B., Skov, L., Hsieh, P., Peyrégne, S., Reher, D., Hopfe, C., Nagel, S., Maricic, T., Fu, Q., Theunert, C., Rogers, R., Skoglund, P., Chintalapati, M., Dannemann, M., Nelson, B.J., Key, F.M., Rudan, P., Kučan, Ž., Gušić, I., Golovanova, L.V., Doronichev, V.B., Patterson, N., Reich, D., Eichler, E.E., Slatkin, M., Schierup, M.H., Andrés, A.M., Kelso, J., Meyer, M., Pääbo, S., 2017. A high-coverage Neandertal genome from Vindija Cave in Croatia. *Science* 358, 655–658.
- Ragsdale, A.P., Weaver, T.D., Atkinson, E.G., Hoal, E.G., Moller, M., Henn, B.M., Gravel, S., 2023. A weakly structured stem for human origins in Africa. *Nature* 617, 755–763.
- Rennie, C.O., Haffajee, M.R., Satyapal, K.S., 2017. Development of the paranasal air sinuses in a South African population utilizing three-dimensional (3D) reconstructed models. *Eur. J. Anat.* 21, 197–209.

- Rightmire, G.P., 1978. Florisbad and human population succession in southern Africa. *Am. J. Phys. Anthropol.* 48, 475–486.
- Rightmire, G.P., 1984. *Homo sapiens* in sub-Saharan Africa. In: Smith, F.H., Spencer, F. (Eds.), *The Origins of Modern Humans: A World Survey of the Fossil Evidence*. Liss, New York, pp. 295–325.
- Rightmire, G.P., 2009. Middle and later Pleistocene hominins in Africa and Southwest Asia. *Proc. Nat. Acad. Sci. USA* 106, 16046–16050.
- Roksandic, M., Radović, P., Wu, X., Bae, C.J., 2022. Resolving the “muddle in the middle”: the case for *Homo bodoensis* sp. nov. *Evol. Anthropol.* 31, 20–29.
- Rothschild, B.M., Zdilla, M.J., Jellema, L.M., Lambert, H.W., 2021. *Cribrra orbitalia* is a vascular phenomenon unrelated to marrow hyperplasia or anemia: paradigm shift for *cribrra orbitalia*. *Anat. Rec.* 304, 1709–1716.
- Scally, A., Durbin, R., 2012. Revising the human mutation rate: implications for understanding human evolution. *Nat. Rev. Genet.* 13, 745–753.
- Scerri, E.M., Drake, N.A., Jennings, R., Groucutt, H.S., 2014. Earliest evidence for the structure of *Homo sapiens* populations in Africa. *Quat. Sci. Rev.* 101, 207–216.
- Scerri, E.M., Thomas, M.G., Manica, A., Gunz, P., Stock, J.T., Stringer, C., Grove, M., Groucutt, H.S., Timmermann, A., Rightmire, G.P., d’Errico, F., 2018. Did our species evolve in subdivided populations across Africa, and why does it matter? *Trends Ecol. Evol.* 33, 582–594.
- Schiffels, S., Durbin, R., 2014. Inferring human population size and separation history from multiple genome sequences. *Nat. Genet.* 46, 919–925.
- Schlebusch, C.M., Skoglund, P., Sjödin, P., Gattepaille, L.M., Hernandez, D., Jay, F., Li, S., De Jongh, M., Singleton, A., Blum, M.G., Soodyall, H., 2012. Genomic variation in seven Khoe-San groups reveals adaptation and complex African history. *Science* 338, 374–379.
- Schlebusch, C.M., Malmström, H., Günther, T., Sjödin, P., Coutinho, A., Edlund, H., Munters, A.R., Vicente, M., Steyn, M., Soodyall, H., Lombard, M., Jakobsson, M., 2017. Southern African ancient genomes estimate modern human divergence to 350,000 to 260,000 years ago. *Science* 358, 652–655.
- Schlebusch, C. M., Sjödin, P., Breton, G., Günther, T., Naidoo, T., Hollfelder, N., Sjöstrand, A. E., Xu, J., Gattepaille, L. M., Vicente, M., Scofield, D. G., Malmström, H., de Jongh, M., Lombard, M., Soodyall, H., Jakobsson, M., 2020. Khoe-San genomes reveal unique variation and confirm the deepest population divergence in *Homo sapiens*. *Mol. Biol. Evol.* 37, 2944–2954.
- Schwartz, J.H., Tattersall, I., 2003. Florisbad. In: Schwartz, J.H., Tattersall, I. (Eds.), *The Human Fossil Record. Volume 2: Craniodental Morphology of Genus *Homo* (Africa and Asia)*. Wiley-Liss, New York, pp. 79–84.
- Scolan, H., Santos, F., Tillier, A.M., Maureille, B., Quintard, A., 2012. Des nouveaux vestiges néanderthaliens à Las Pélénos (Monsempron-Libos, Lot-et-Garonne, France). *Bull. Mém. So. Anthropol. Paris* 24, 69–95.
- Shore, L.R., 1938. A note on the interparietal groove in Egyptian skulls. *J. Anat.* 73, 1–14.
- Singer, R., 1958. The Rhodesian, Florisbad and Saldanha skulls. In: von Koenigswald, G.H.R. (Ed.), *Hundert Jahre Neanderthaler*. Keminck en Zoon, Utrecht, pp. 52–62.
- Smith, F.H., Falsetti, A.B., Donnelly, S.M., 1989. Modern human origins. *Am. J. Phys. Anthropol.* 32, 35–68.
- Smith, P., Brink, J.S., Hoffman, J.W., Bam, L.C., Nshimirimana, R., de Beer, F.C., 2015. The late Middle Pleistocene upper third molar from Florisbad: metrics and morphology. *Trans. R. Soc. S. Afr.* 70, 233–244.
- Song, S., Sliwerska, E., Emery, S., Kidd, J.M., 2017. Modeling human population separation history using physically phased genomes. *Genetics* 205, 385–395.
- Spoor, F., Stringer, C., Zonneveld, F., 1998. Rare temporal bone pathology of the Singa calvaria from Sudan. *Am. J. Phys. Anthropol.* 107, 41–50.
- Steyn, M., Voeller, S., Botha, D., Ross, A.H., 2016. *Cribrra orbitalia*: prevalence in contemporary populations. *Clin. Anat.* 29, 823–830.
- Stringer, C., 2016. The origin and evolution of *Homo sapiens*. *Phil. Trans. R. Soc. B: Biol. Sci.* 371, 20150237.
- Stringer, C. B., Andrews, P. 1988. Genetic and fossil evidence for the origin of modern humans. *Science* 239, 1263–1268.
- Stringer, C.B., Cornish, L., Stuart-Macadam, P., 1985. Preparation and further study of the Singa skull from Sudan. *Bul. Brit. Mus. Nat. Hist. (Geol.)* 38, 347–358.
- Stuart-Macadam, P., 1987. A radiographic study of porotic hyperostosis. *Am. J. Phys. Anthropol.* 74, 511–520.
- Tappe, N.C., 1987. Circum-mortem damage to some ancient African hominid crania: a taphonomic and evolutionary essay. *Afr. Archaeol. Rev.* 5, 39–47.
- Tobias, P.V., 1968. Middle and early Upper Pleistocene members of the genus *Homo* in Africa. In: Kurth, G. (Ed.), *Evolution und Hominization*, 2nd Edition. Gustav Fischer, Stuttgart, pp. 176–194.
- Toffolo, M.B., 2024. Pleistocene archaeology and environments of the Free State, South Africa. *Azania: Archaeol. Res. Afr.* 59, 317–351.
- Veeramah, K.R., Hammer, M.F., 2014. The impact of whole-genome sequencing on the reconstruction of human population history. *Nat. Rev. Genet.* 15, 149–162.
- Veeramah, K.R., Wegmann, D., Woerner, A., Mendez, F.L., Watkins, J.C., Destro-Bisol, G., Soodyall, H., Louie, L., Hammer, M.F., 2012. An early divergence of KhoeSan ancestors from those of other modern humans is supported by an ABC-based analysis of autosomal resequencing data. *Mol. Biol. Evol.* 29, 617–630.
- Wells, L.H., 1951. The fossil human skull from Singa. In: Arkell, A.J., Bate, D.M.A., Wells, L.H., Lacaille, A.D., *The Pleistocene Fauna of Two Blue Nile Sites: Fossil Mammals of Africa, No.2*. British Museum of Natural History, London, pp. 29–42.
- Woodward, A.S., 1938. A fossil skull of an ancestral Bushman from the Anglo-Egyptian Sudan. *Antiquity* 12, 193–195.
- Zdilla, M.J., Nestor, N.S., Rothschild, B.M., Lambert, H.W.,

2022. Cribra orbitalia is correlated with the meningo-orbital foramen and is vascular and developmental in

nature. *Anat. Rec.* 305, 1629–1671.

Supplement 1: Revisiting the Anatomy of the Florisbad Hominin Cranium: Visualization of New Internal Features and Observations on Its Supposed Pathologies

ANTOINE BALZEAU

PaleoFED team, UMR 7194, Histoire Naturelle de l'Homme Préhistorique, MNHN-CNRS-UPVD, Paris, FRANCE; and, Department of African Zoology, Royal Museum for Central Africa, Tervuren, Belgium; antoine.balzeau@mnhn.fr

JIAMING HUI

PaleoFED team, UMR 7194, Histoire Naturelle de l'Homme Préhistorique, MNHN-CNRS-UPVD, Paris, FRANCE; Key Laboratory of Vertebrate Evolution and Human Origins, Institute of Vertebrate Paleontology and Paleoanthropology, Chinese Academy of Sciences, Beijing 100044, CHINA; and, Sorbonne Université, Paris, FRANCE; jiaming.hui@etu.sorbonne-universite.fr

VICTOR GIOLLAND

PaleoFED team, UMR 7194, Histoire Naturelle de l'Homme Préhistorique, MNHN-CNRS-UPVD, Paris, FRANCE; victor.giolland@mnhn.fr

SHARON HOLT

Florisbad Quaternary Research Station, National Museum, Bloemfontein, 9301, SOUTH AFRICA; sholt@nationalmuseum.co.za

FREDERICK GRINE

Department of Anthropology and Department of Anatomical Sciences, Renaissance School of Medicine, Stony Brook University, Stony Brook, New York 11794, USA; frederick.grine@stonybrook.edu

SUPPLEMENT 1

This supplement includes: supplementary information table S1.

Table S1. THE INVENTORY OF FOSSIL SPECIMENS INCLUDED IN COMPARATIVE ANALYSES.
Data for comparative specimens are from our previously published papers (Balzeau 2013; Balzeau et al. 2022; Hui and Balzeau 2023).

Specimen	Taxon	Comparative analyses
TM 266-01-060-1	<i>Sahelanthropus tchadensis</i>	FS
Sts 5	<i>Australopithecus africanus</i>	FS; Endo
Sts 60	<i>A. africanus</i>	Endo
Sts 71	<i>A. africanus</i>	FS
StW 505	<i>A. africanus</i>	FS
StW 573	<i>A. prometheus?</i>	FS
BOU-VP-12/130	<i>A. garhi</i>	FS
U.W. 88-50	<i>A. sediba</i>	FS
KNM-WT 17000	<i>Paranthropus aethiopicus</i>	FS
SK 48	<i>P. robustus</i>	FS
DNH 155	<i>P. robustus</i>	FS
OH 5	<i>P. boisei</i>	FS
KNM-ER 13750	<i>P. boisei</i>	Endo
ER23000	<i>P. boisei</i>	Endo
STW 53	<i>Australopithecus?</i>	FS
KNM-ER 1805	<i>H. habilis</i>	Endo
KNM-ER 1813	<i>H. habilis</i>	Endo
OH 16	<i>H. habilis</i>	Endo
KNM-ER 3733	<i>H. erectus</i>	Endo; CVT
KNM-ER 3883	<i>H. ergaster / H. erectus</i>	FS; Endo; CVT
OH 9	<i>H. erectus</i>	FS
D2280	<i>H. erectus / H. georgicus</i>	FS
D2282	<i>H. erectus / H. georgicus</i>	FS
D2700	<i>H. erectus / H. georgicus</i>	FS
D3444	<i>H. erectus / H. georgicus</i>	FS
D4500	<i>H. erectus / H. georgicus</i>	FS
Trinil 2	<i>H. erectus</i>	FS; CVT
Hexian	<i>H. erectus</i>	CVT
Zhoukoudian 1	<i>H. erectus</i>	Endo
Zhoukoudian 2	<i>H. erectus</i>	Endo
Zhoukoudian 3	<i>H. erectus</i>	Endo
Zhoukoudian 10	<i>H. erectus</i>	Endo
Zhoukoudian 12	<i>H. erectus</i>	Endo
Sangiran 2	<i>H. erectus</i>	Endo; CVT
Sangiran 17	<i>H. erectus</i>	FS; Endo
Skull IX	<i>H. erectus</i>	FS
Sambungmacan 1	<i>H. erectus</i>	CVT
Sambungmacan 3	<i>H. erectus</i>	Endo
Sambungmacan 4	<i>H. erectus</i>	FS
Ngandong 1	<i>H. erectus</i>	FS; CVT

Ngandong 5	<i>H. erectus</i>	Endo
Ngandong 7	<i>H. erectus</i>	FS; CVT; Endo
Ngandong 12	<i>H. erectus</i>	FS; CVT; Endo
Ngawi 1	<i>H. erectus</i>	FS; CVT
Lesedi 1	<i>H. naledi</i>	FS
Broken Hill 1	<i>H. heidelbergensis?</i>	FS; CVT; Endo
TD6-15	<i>H. antecessor</i>	FS
HK 87	?	FS
Bodo	<i>H. heidelbergensis?</i>	FS
Ehringsdorf H1024	?	FS
Ehringsdorf H1025	?	FS
Petralona	<i>H. heidelbergensis?</i>	FS; CVT
Ceprano	<i>H. heidelbergensis?</i>	FS
Aroeira	<i>H. heidelbergensis?</i>	FS
SHS 5	?	FS
SHS 12	?	FS
SHS 13	?	FS
SHS 15	?	FS
SHS 17	?	FS
Steinheim	<i>H. heidelbergensis?</i>	FS
Zuttiyeh	?	FS
Feldhofer	<i>H. neanderthalensis</i>	FS
Neandertal	<i>H. neanderthalensis</i>	Endo
Saccopastore	<i>H. neanderthalensis</i>	Endo; CVT
La Ferrassie 1	<i>H. neanderthalensis</i>	FS; CVT; DV; Endo
La Quina H5	<i>H. neanderthalensis</i>	FS; CVT; DV; Endo
Guattari	<i>H. neanderthalensis</i>	FS; CVT
Forbes' Quarry 1	<i>H. neanderthalensis</i>	FS
Krapina 3	<i>H. neanderthalensis</i>	FS
Krapina 6	<i>H. neanderthalensis</i>	FS
La Chapelle-aux-Saints 1	<i>H. neanderthalensis</i>	FS; CVT; DV; Endo
Spy 1	<i>H. neanderthalensis</i>	FS; CVT; DV; Endo
Spy 10	<i>H. neanderthalensis</i>	FS; CVT; DV; Endo
Amud	<i>H. neanderthalensis</i>	FS
Apidima 2	<i>H. neanderthalensis</i>	FS
Monte Circe	<i>H. neanderthalensis</i>	Endo
Tabun C1	<i>H. neanderthalensis</i>	FS; Endo
LH 18	?	FS; Endo
Jebel Irhoud 1	?	FS; Endo
Qafzeh 9	<i>H. sapiens</i>	FS
Hofmeyr	<i>H. sapiens</i>	FS
Cro Magnon 1	<i>H. sapiens</i>	FS; CVT; DV; Endo
Cro Magnon 2	<i>H. sapiens</i>	FS; CVT; DV
Cro Magnon 3	<i>H. sapiens</i>	FS; CVT; DV
Abri Pataud 1	<i>H. sapiens</i>	FS; CVT; DV; Endo

Afalou 2, 30, 34	<i>H. sapiens</i>	FS
Afalou 2, 12, 13, 28, 30, 34	<i>H. sapiens</i>	CVT
Taforalt XI C1, XV C4, XV C5	<i>H. sapiens</i>	FS
Taforalt XI C1, XII C1, XV C2, XV C4, XV C5, XVII C1	<i>H. sapiens</i>	CVT
Rochereil	<i>H. sapiens</i>	CVT
Song Terus	<i>H. sapiens</i>	CVT
Skhul 5	<i>H. sapiens</i>	Endo; CVT
Predmost 3	<i>H. sapiens</i>	Endo
Predmost 4	<i>H. sapiens</i>	Endo
Predmost 9	<i>H. sapiens</i>	Endo
Predmost 10	<i>H. sapiens</i>	Endo
Dolní Věstonice 1	<i>H. sapiens</i>	Endo
Brno 3	<i>H. sapiens</i>	Endo
Téviec 8	<i>H. sapiens</i>	CVT
Téviec 9	<i>H. sapiens</i>	CVT
Téviec 16	<i>H. sapiens</i>	CVT

Note: FS: frontal sinus; CVT: cranial vault thickness; DV: diploic venous system; Endo: endocast.